Somatodendritic Expression of JAM2 Inhibits Oligodendrocyte Myelination

Somatodendritic Expression of JAM2 Inhibits Oligodendrocyte Myelination

Stephanie A. Redmond[1], Feng Mei[1], Yael Eshed-Eisenbach[2], Lindsay A. Osso[1], Dena Leshkowitz[3], Yun-An A. Shen[1], Jeremy N. Kay[4], Michel Aurrand-Lions[5], David A. Lyons[6], Elior Peles[2]* and Jonah R. Chan[1]*

[1] Department of Neurology and Program in Neuroscience, University of California, San Francisco, San Francisco, California, USA.
[2] Department of Molecular Cell Biology, The Weizmann Institute of Science, Rehovot, Israel.
[3] Bioinformatics Unit, Department of Biological Services Weizmann Institute of Science, Rehovot, Israel.
[4] Duke University School of Medicine, Departments of Neurobiology and Ophthalmology, Durham, North Carolina, USA
[5] Centre de Recherche en Cancérologie de Marseille, Inserm, CNRS, Aix-Marseille University, UMR1068, Marseille, France
[6] Centre for Neuroregeneration, Centre for Multiple Sclerosis Research, Euan MacDonald Centre for Motor Neurone Disease Research, University of Edinburgh, Edinburgh, UK.

*To whom correspondence should be addressed:
Dr. Jonah R. Chan
Department of Neurology and Program in Neuroscience
University of California San Francisco
Sandler Neurosciences Center
675 Nelson Rising Lane, Rm. 214C, Box 3206
San Francisco, CA 94158
Tel.: 415-514-9818
Email: jonah.chan@ucsf.edu

Dr. Elior Peles
Department of Molecular Cell Biology
Wolfson Building for Biological Research
Room 115
Weizmann Institute of Science
Rehovot 7610001, Israel
Tel.: +972-8-934-4561
Email: peles@weizmann.ac.il

Myelination occurs selectively around neuronal axons to increase the efficiency and velocity of action potentials. While oligodendrocytes are capable of myelinating permissive structures in the absence of molecular cues, structurally permissive neuronal somata and dendrites remain unmyelinated. Utilizing a purified spinal cord neuron-oligodendrocyte myelinating coculture system, we demonstrate that disruption of dynamic neuron-oligodendrocyte signaling by chemical crosslinking results in aberrant myelination of the somatodendritic compartment of neurons. We hypothesize that an inhibitory somatodendritic cue is necessary to prevent non-axonal myelination. Using next-generation sequencing and candidate profiling, we identify neuronal Junction Adhesion Molecule 2 (JAM2) as an inhibitory myelin-guidance molecule. Taken together, our results demonstrate that the somatodendritic compartment directly inhibits myelination, and suggest a model in which broadly indiscriminate myelination is tailored by inhibitory signaling to meet local myelination requirements.

The central nervous system (CNS) greatly benefits from oligodendrocyte myelination. Myelin supports the clustering of ion channels to nodes of Ranvier and increases the resistance across the axonal membrane. These properties generate the saltatory conduction of action potentials, ensuring rapid and efficient neural communication over longer distances in a more compact space (Zalc et al., 2008). It has long been appreciated that myelin, with very few exceptions, forms selectively around axons (Braak et al., 1977; Lubetzki et al., 1993; Blinzinger et al., 1972; Remahl and Hildebrand, 1985; Cooper and Beal, 1977). This begs the fundamental question: how does an oligodendrocyte, the myelin-forming cells of the CNS, target each of its many myelin segments exclusively to axons?

Very little is currently known about axon selection by oligodendrocytes. More well understood are the consequences of when myelin fails to form correctly around axons, such as in leukodystrophies, or when myelin is attacked by the immune system, as in multiple sclerosis. In such cases, neuronal function is impaired and neurons eventually degenerate if myelin is not reformed (Fancy et al., 2011; Franklin and ffrench-Constant, 2008; Trapp and Nave, 2008; Yuen et al., 2014). In development, the coordinated differentiation and myelination of thousands of spatially distributed oligodendroglia is thought to be extrinsically determined, perhaps by neuronal activity. Indeed, recent findings suggest that neuronal activity is involved in modulating axon selection and the extent of myelin segment formation (Gibson, 2014; Hines et al., 2015; Mensch et al., 2015).

An unexplored aspect of myelination is the avoidance of selecting non-axonal targets. In CNS gray matter, oligodendrocytes must select axons while avoiding neuronal cell bodies, dendrites and processes of other glial cells. How is this specificity accomplished? Little evidence of non-axonal oligodendrocyte myelination exists (Blinzinger et al., 1972; Braak et al., 1977). Curiously, *in vitro*, oligodendrocyte myelination is not limited to axons: oligodendrocytes produce myelin membranes on planar glass coverslips, cylindrical polystyrene nanofibers (Bechler et al., 2015; Lee et al., 2012), and conical glass micropillars (Mei et al., 2014). These observations suggest that myelin substrate selection is not cell-

intrinsically limited to physiologically relevant axon-like geometries, and that an inductive cue is not strictly required for differentiation and myelination. Oligodendrocyte cell processes are thus likely sensitive to cell-extrinsic 'myelin guidance' cues that ensure only correct selection of pre-myelinated axons.

We propose three potential mechanisms that would ensure correct axonal selection (Fig 1a). An attractive signal may be expressed by the neuronal axon (Fig 1a, 'Attraction') to specifically promote myelin formation. Alternatively, proper myelination of axons may be achieved by expression of an inhibitory cue by the neuron's somatodendritic compartment (Fig 1a, 'Inhibition'). Here, oligodendrocyte processes form myelin segments around permissive axons but not on inhibitor-expressing structures. However, the Attraction and Inhibition models are not mutually exclusive, and both modes of signaling may be at play to ensure proper targeting of myelin segments (Fig 1a, 'Mixed'). Which of these signaling mechanisms are active during developmental myelination? By utilizing a purified spinal cord neuron-oligodendrocyte myelinating coculture system, we demonstrate that disruption of dynamic neuron-oligodendrocyte signaling results in aberrant myelination of the somatodendritic compartment of neurons indicative of an active inhibitory mechanism. Using next-generation sequencing and candidate profiling, we identify Junction Adhesion Molecule 2 (JAM2) as a somatodendritic protein necessary and sufficient to inhibit oligodendrocyte myelination. Taken together, our results demonstrate that the somatodendritic compartment directly inhibits myelination, and provide a model in which broadly indiscriminate myelination is tailored by inhibitory signaling to meet local myelination requirements.

Results

The somatodendritic compartment is biophysically permissive to myelin ensheathment

To understand the nature of selectivity and fidelity of the myelination process, we reasoned that the presence of a somatodendritic inhibitor would only be required if oligodendrocytes are capable of ensheathing the spherical shape of a neuron cell body (Fig 1b). To test this possibility, we cultured primary rat oligodendrocyte precursor cells (OPCs) on nanofibers with 20-micrometer diameter polystyrene beads that mimic neuron cell body geometry (Fig 1c). We find that differentiated myelin basic protein-positive (MBP+) oligodendrocytes readily ensheathe myelin membranes around both nanofibers and beads (Fig 1d).

We then asked whether the somatodendritic compartment remains unmyelinated due to lack of attraction, or expression of inhibition? To investigate this question, we developed a primary purified spinal cord neuron (SCN) and oligodendroglial myelinating coculture system (Fig 1b,e-i). The SCN cultures robustly exhibited extensive axons, dendrites, and formed neuronal synapses over the course of three weeks *in vitro* (Fig 1e-g). Under normal conditions, purified OPCs seeded onto mature SCN cultures proliferate, differentiate after approximately one week *in vitro* (Fig 1h-i), and form compact layers of myelin membrane around axons (Fig 1j). Oligodendrocytes wrap myelin membrane around axons while avoiding neuron somata and dendrites (Fig 2a) (Lubetzki et al., 1993), recapitulating gray matter myelination patterns *in vitro*. We then asked whether dynamic neuron-oligodendrocyte signaling is

required to prevent myelination of the somatodendritic compartment. Prior to seeding neuron cultures with OPCs, we treated the neurons with the chemical cross-linker paraformaldehyde (PFA) (Rosenberg et al., 2008). Surprisingly, oligodendrocytes wrapped myelin membranes on fixed neuron somata and dendrites in addition to axons (Fig 2b-c), and form multiple compacted layers of myelin membrane around cellular processes (Fig 2d-e). It is important to note, that paraformaldehyde cross-linking and the extended period of coculturing, subcellular structures are not well maintained (Rosenberg et al., 2008), making it impossible to determine whether myelinated structures are axons or dendrites. Based on our observations that (1) cultured oligodendroglia ensheathe bare nanofibers and microbeads, (2) avoid ensheathing neural somatodendritic compartments *in vitro* and *in vivo*, yet (3) aberrantly ensheathe cross-linked somata and dendrites, we hypothesize that neurons must express inhibitory molecules to prevent somatodendritic myelination.

Differential RNA-seq and candidate profiling for myelination-inhibitory molecules

To identify candidate inhibitory molecules, we conducted next-generation RNA-sequencing of SCN as well as dorsal root ganglion neuron (DRG) cultures (Fig 3a). We reasoned that differential expression analysis would increase the likelihood of identifying a somatodendritic inhibitor of myelination because SCN cultures develop extensive dendritic arbors around their somata, while pseudo-unipolar DRG neurons lack true dendrites. Candidate inhibitory proteins were chosen based on the following criteria: proteins that have (1) significantly higher expression in SCNs as compared to DRGs, and (2) transmembrane domains (Fig 3b). The differential RNA-seq analysis yielded two distinct populations of transcripts, representing higher expression in either DRGs (Fig 3b-d, black) or SCNs (Fig 3b-d, dark gray/pink). Several genes that have been described in the literature as expressed in either DRGs or SCNs were also differentially expressed in our analysis (Fig 3d, black and gray bars). Overall, 170 unique genes were identified as candidate inhibitory proteins (Fig 3b-d, pink). By profiling and prioritizing candidates from the RNAseq analysis, we identified the protein Junction Adhesion Molecule 2 (JAM2) as a differentially expressed (Fig 3d-e) potential inhibitor of myelination because of its low expression in DRG somata (Fig 3f, insert), little to no expression in the majority of DRG (Fig 3f) and SCN axons (Fig 3g), and its high expression and specific localization on the somatodendritic compartment of SCN (Fig 3g).

JAM2 is sufficient to inhibit oligodendroglial wrapping

JAM2 is a single-pass transmembrane protein with two extracellular immunoglobulin-like domains (Arcangeli et al., 2013). We found that the extracellular portion of JAM2 fused to the Fc region of immunoglobulins ('JAM2-Fc') strongly binds to MBP-positive oligodendrocytes and weakly to PDGF receptor alpha-positive (PDGFRα+) OPCs (Fig 4a) compared to an Fc only negative control (Fig 4b). This suggests that oligodendroglia express at least one JAM2 receptor, and the expression of JAM2 receptor(s) is upregulated as oligodendroglia differentiate. We hypothesized that if JAM2 acts to inhibit myelination, oligodendrocytes will avoid wrapping JAM2-coated permissive structures *in vitro.* To test this

possibility, we adapted the micropillar array platform (Mei et al., 2014) (Fig 4c) to assay the activity of Fc-fusion proteins on oligodendroglial wrapping. Wildtype OPCs were seeded onto micropillars coated with either JAM2-Fc or Fc alone. Under control conditions, OPCs and oligodendrocytes associate with micropillars and wrap them with PDGFRα+ or MBP+ membranes. When a single optical section is taken through the micropillar array, immunostained OPC and oligodendrocyte wrapping is visualized as a ring (Figure 4d). Compared to Fc alone, oligodendrocytes wrap significantly fewer JAM2-Fc coated micropillars (Fig 4e-h, 85.7% reduction). Interestingly, even OPC wrapping of micropillars is significantly reduced in the JAM2-Fc condition compared with Fc alone (Fig 4h; 66.6% reduction). We reasoned that we might observe a decrease in OPC and oligodendrocyte wrapping if oligodendroglia failed to adhere or differentiate on JAM2-Fc coated surfaces. Due to technical limitations of imaging cells within the micropillar fields, we quantified the densities of OPCs and oligodendrocytes on JAM2-Fc or Fc coated areas directly adjacent to the micropillar arrays. We found no significant difference between the densities of OPCs or oligodendrocytes between JAM2-Fc and Fc conditions (Fig 4i). Taken together, these results show that the extracellular portion of JAM2 is sufficient to specifically inhibit oligodendroglial wrapping without affecting cell density or oligodendrocyte differentiation.

JAM2 is necessary to prevent somatodendritic myelin wrapping

Given that oligodendrocytes wrap nanofibers, beads, and Fc coated micropillars, but significantly fewer JAM2-Fc coated micropillars, we next asked whether JAM2 signaling is sufficient to inhibit myelin segment formation *in vitro*. We established myelinating SCN cocultures in the presence of either soluble Fc or JAM2-Fc. After seven days, the cocultures were immunostained for MBP and Fc, and the number of MBP+ segments per oligodendrocyte was analyzed. Consistent with Fc binding analysis, myelinating oligodendrocytes in the control condition do not show specific Fc labeling (Fig 5a), while oligodendrocytes in the JAM2-Fc condition show co-labeling of MBP and JAM2-Fc (Fig 5b), indicating that myelinating oligodendrocytes express a JAM2 receptor. Interestingly, we find that the number MBP+ segments formed per oligodendrocyte is significantly reduced in the presence of JAM2-Fc as compared to Fc alone (Fig 5c, 24.6% reduction).

Next, we investigated whether JAM2 is necessary to prevent somatodendritic myelin wrapping of SCNs. First, we established myelinating cocultures with wildtype SCN and OPCs, and allowed them to interact normally for five days *in vitro*. During the final two days of coculture, at the onset of OPC differentiation and initiation of myelination, we applied a function-blocking antibody against JAM2 (Fig S1a-c). In control conditions, oligodendrocyte segments are overwhelmingly wrapped on axons (Fig S1a). However, in the presence of JAM2 function-blocking antibody, we found that oligodendrocytes wrap significantly more MBP+ segments on neuronal dendrites (Fig S1b-c, 321.8% increase).

To understand whether neuronal JAM2 is necessary to ensure that the somatodendritic compartment remains unmyelinated, we established myelinating cocultures with wildtype OPCs and either JAM2-knockout (JAM2 KO) or wildtype (WT) SCNs. We observed that compared to wildtype SCN controls (Fig

5d), wildtype oligodendrocytes wrapped significantly more MBP+ segments on JAM2-deficient somatodendritic compartments (Fig 5e-f, 226.4% increase). Strikingly, we frequently observed large spheroidal 'bubbles' of MBP+ membranes in JAM2 KO neuron cocultures (Fig 5e, MBP panel arrowheads). These structures stood out against the typically cylindrical myelin segments on axons and colocalized with neuronal somata (Fig 5e, MAP2 panel arrowheads). We quantified the relative frequency in which neuron cell bodies are wrapped with myelin membranes, and find that JAM2-knockout somata are five-fold more likely to be wrapped by oligodendrocytes compared with wildtype controls (Fig 5g).

During normal axonal myelination, oligodendrocyte adhesion proteins cause the clustering of neuronal proteins and ion channels to nodes of Ranvier, enabling saltatory conduction of action potentials. We next asked whether aberrant somatic wrapping could affect the molecular organization of JAM2-knockout neurons? Unexpectedly, we observe that MBP+ membrane wrapping of neuronal somata induced the clustering of neuronal contactin-associated protein (CASPR) (Fig S2a, inset 1). Wrapped neuronal dendrites also exhibited clustered CASPR (Fig S2a, inset 2), but unwrapped somata and dendrites showed no CASPR clusters (Fig S2a, inset 3). This pattern of molecular organization is indicative of a direct neuroglial molecular interaction normally restricted to paranodes at the node of Ranvier (Einheber et al., 1997; Eisenbach et al., 2009; Pedraza et al., 2009).

Loss of JAM2 results in myelination of the somatodendritic compartment *in vivo*

In the more complex environment of the CNS, is inhibitory JAM2 signaling required to prevent myelination of the somatodendritic compartment? At postnatal day 30-31 (P30-31) in the mouse, most neurons in the cervical spinal cord express JAM2. We examined a JAM2 reporter and JAM2 protein expression in spinal cord cross-sections of both *jam2*:beta-galactosidase knock-in mice (Fig S3a-b), as well as heterozygous and JAM2 KO mice, respectively (Fig S3c-d, Fig S4a-b;). The CNS is heavily myelinated and individual myelin segments are generally difficult to resolve by immunostaining. One exception to this technical limitation is the dorsal horn, where very few axons are myelinated. In this area, we observed many beta-galactosidase/NeuN-positive neurons (Fig S3a), and robust gray matter JAM2 immunostaining in heterozygous but not JAM2 KO mice (Fig S4a-b), confirming the specificity of the antibody staining. In P31 littermate wildtype and JAM2 KO mice, we found no significant differences in the average densities of NeuN-positive neurons or CC1-positive oligodendrocytes within the dorsal horn region (Fig S3c-f), suggesting that the development of these two cell types is normal in the absence of JAM2.

When we examined myelination patterns in dorsal horns of littermate wildtype and JAM2 KO mice (Fig 6a-d), we observed conspicuous MBP+ membrane 'bubbles' around neuronal somata in JAM2 KO dorsal horns (Fig 6c-d, arrowheads). Seventy-two percent of JAM2 KO hemisections contained more than one myelin-wrapped neuron, compared to just 16% of wildtype hemisections (Fig 6e). Overall, the median number of wrapped neurons per hemisection was four-fold higher in JAM2 KO mice compared to wildtype littermates (Figure 6f). Optical sectioning of immunostained tissue revealed that wrapped neurons could be wrapped with MBP-positive membrane around their entire circumference through several micrometers

in the z-axis (Fig 6g), reminiscent of myelin-wrapped beads (Fig 1d). One of the hallmarks of myelination is the clustering of CASPR to paranodes. Like myelin-wrapped JAM2 KO neurons *in vitro* (Fig S2a), we find that the molecular organization of CASPR on JAM2 KO neurons is dramatically affected by somatic myelination *in vivo.* CASPR protein clustering is evident on MBP+ membrane-wrapped JAM2-knockout neurons (Fig S2b). Consistent with our immunostaining observations, semi-thin sections through a JAM2 KO dorsal horn neuron show myelination around the total circumference of a soma (Fig 6h). This particular cell is wrapped across three different semi-thin sections (Fig S2c-e).

We wanted to further understand the identity of the wrapped Jam2-knockout neurons. Based on our observations that Jam2-knockout neurons are generally wrapped around their entire circumference *in vivo*, are small (10-20 micrometer diameter) and have little cytoplasm (Fig 6c,d,g-h; Fig S2b-c), we screened dorsal horn interneuron markers, and found that MBP+ wrapped neurons are exclusively positive for the paired box gene 2 (PAX2) transcription factor (Figure 7a-e). PAX2+ dorsal horn neurons are inhibitory interneurons and their dendrites and axons exhibit islet morphology oriented along the rostral-caudal axis of the spinal cord (Smith et al., 2015). We find that approximately six-percent of PAX2+ neurons are wrapped in JAM2-knockout mice, significantly more than the under two-percent observed in JAM2-heterozygous mice (Fig 7f). We find no difference in the density of PAX2+ neurons in the dorsal horn between genotypes (Fig 7g). Finally, we find that PAX2+ neurons receive very little presynaptic innervation of their somata (Fig S5a-b) with many cells of both genotypes exhibiting no presynaptic puncta (VGLUT1: 64.4%; VGLUT2: 23.3%; VGAT: 30.6%). We also never observed synaptic puncta between the wrapping MBP+ sheath and the PAX2+ neuron cell body (Fig S5c, 0/480 PAX2+ neurons). Taken together, our observations support the conclusion that oligodendrocyte myelin membranes are in direct contact with neural somata as they wrap.

Discussion

Overall, we show that somatodendritic JAM2 is necessary and sufficient to inhibit oligodendrocyte wrapping. Our results support a model of myelin target selection and wrapping in which pre-myelinating oligodendrocyte processes (Fig 8a) are normally inhibited by somatodendritic cues, including JAM2 (Fig 8b). When such inhibitors are missing, as in JAM2 KO mice, oligodendrocytes form aberrant somatodendritic myelin wraps (Fig 8c). As growing neurons utilize both attractive and repulsive axon guidance cues to precisely target correct brain areas and postsynaptic neurons, our findings indicate that oligodendrocytes utilize somatodendritic inhibition, potentially in addition to axonal attraction, to target myelin segments specifically to axons (Fig 1a, ‘Inhibition’, ‘Mixed’).

Inhibitory signals guide oligodendrocyte myelination

The need for inhibitory signaling in tailoring myelination patterns becomes more apparent in neuron-free myelination assays. When oligodendroglia are cultured in the presence of permissive nanofibers, micropillars and spherical beads, they wrap MBP+ myelin membranes around each structure type,

including the 50-micrometer diameter circular base of a micropillar (Figs 1c-d, 4c). These results suggest that oligodendroglia have few geometric requirements to form myelin. Indeed, the study of myelination by culturing oligodendrocytes on planar glass coverslips has historically been a successful approach because the cells readily differentiate and form membrane sheets with myelin-like composition in the absence of inductive substrate signaling. Here we use the oligodendrocyte's flexible wrapping requirements to our advantage by adapting the high-throughput micropillar array platform to screen integral membrane protein activity on oligodendrocyte wrapping (Fig 4c-i). Under identical geometric conditions, and in the absence of any other molecular cues, oligodendrocytes and OPCs are dramatically less likely to wrap micropillars coated with JAM2-Fc (Fig 4e-h), and oligodendrocytes form significantly fewer myelin segments in the presence of soluble JAM2-Fc (Fig 5a-c). Interestingly, the magnitude of JAM2 inhibition is greater on micropillars (66.6%) than in SCN cocultures (24.6%), opening the possibility that axons may express an attractive signal that is able to partially overcome JAM2 inhibition. These results demonstrate the sufficiency of JAM2 to inhibit wrapping, and support the model that oligodendroglial target selection can be regulated by negative and positive microenvironment cues (Fig 1a 'Mixed').

Furthermore, JAM2's inhibition of wrapping is not the result of changes in oligodendroglial cell density or differentiation (Figs 4i; S4c-f). In contrast, previously described inhibitors of axonal myelination negatively affect oligodendroglial cell adhesion *in vitro* and/or oligodendrocyte differentiation *in vitro* and *in vivo* (e.g. LINGO-1, LSAMP) (Lee et al., 2007; Mi et al., 2005; Sharma et al., 2015). It would not necessarily be advantageous for an inhibitor of somatodendritic myelination to prohibit oligodendrocyte differentiation. Oligodendrocytes would still need to differentiate and myelinate gray matter axons that are tightly intermingled with neuron cell bodies and dendrites.

Additional inhibitory myelin guidance molecules

What additional signal(s) prevent aberrant wrapping of other spinal cord neurons and dendrites? JAM2 is widely expressed in the young adult mouse spinal cord (Figs S3, S4a-b). Here we describe the aberrant wrapping of dorsal horn neuron cell bodies. Additional EM analysis of heavily myelinated gray matter areas may reveal that other neuron somatodendritic compartments are wrapped in JAM2 KO mice that are not detectable by immuno- or toluidine blue staining. Nevertheless, it is entirely possible that other neuron types may express other inhibitory molecules in addition to, or instead of JAM2. But even among JAM2-expressing spinal cord motor neurons, it is notable that their dendrites and cell bodies are densely covered with presynaptic terminals (Molofsky et al., 2014), another normally unmyelinated neuronal structure. Axon terminals, then, may present either a structural barrier preventing oligodendroglial contact with somatodendritic surfaces, or may themselves express a myelination-inhibitory cue that is sufficient to prevent oligodendrocyte wrapping with or without somatodendritic expression of JAM2. Unlike ventral motor neurons, dorsal horn PAX2+ neurons are largely devoid of presynaptic innervation of their somata (Fig S5). Importantly, our data does not distinguish between the possibilities that somatic myelin wrapping

removes synapses, or whether only neurons devoid of somatic synaptic terminals are vulnerable to myelin wrapping in the absence of JAM2. In addition to neural sources of myelin inhibition, astrocytes, microglia, oligodendroglia and endothelial cells also remain unmyelinated, and may each express a molecular cue to prevent wrapping.

Oligodendroglial JAM2 receptors

Many receptors in oligodendroglia may be responsible for transducing myelin guidance signals, especially if JAM2 is one of many inhibitory molecules in the CNS. Known JAM2 receptors include other JAM family members JAM1, 2 and 3, as well as integrin alpha-4 beta-1, which may act alone or in combination to bind JAM2 (Arcangeli et al., 2013). In this study, the identity of the JAM2 receptor(s) in oligodendrocytes remains an open question. But if oligodendrocyte differentiation and wrapping are indeed dissociable events as our results suggest (Fig 4e-i), the understanding of downstream mechanisms that separately govern these two processes will be of high interest for future study.

Inhibitory myelin guidance molecules and failure of myelin repair

Promoting efficient myelin repair in diseases like multiple sclerosis (MS) has long been a clinical goal. While current therapies aim to control immune infiltration into the CNS, more attention is now being given to directly promoting oligodendrocyte differentiation and remyelination (Mei et al., 2014; Ruckh et al., 2012). However, it has also been observed in human postmortem MS lesions that differentiated oligodendrocytes are present, but fail to remyelinate axons (Chang et al., 2002). Could inhibitory myelin guidance molecules be aberrantly upregulated or mislocalized in MS lesions and prevent efficient repair? If so, it is essential to identify such signals, as they may be feasible targets to block and promote myelin repair. As additional myelin guidance molecules are identified, it will be important to understand their roles in both myelin formation and regeneration.

Experimental Procedures

Animals

All animals used in this study were housed and handled with the approval of the University of California San Francisco Institutional Animal Care and Use Committee (IACUC). Timed-pregnant Sprague-Dawley rats were procured from Jackson Laboratory. Dorsal root ganglion neuron and spinal cord neuron dissections were done on embryonic day 15. Junction Adhesion Molecule 2 (JAM2) knockout mice are as previously described (Arcangeli et al., 2011). The *jam2:beta-galactosidase* knock-in mice were purchased from Jackson Laboratory ($Jam2^{tm1.1(KOMP)Mbp}$). Jam2 knockout mice were used to generate data in Figures 5-6, S3-S4, and $Jam2^{tm1.1(KOMP)Mbp}$ mice were used to generate data in Figures 7, S2 and S5.

Immunohistochemistry

Cell cultures were immunostained with standard techniques, discussed elsewhere in detail (Lee et al., 2013). Briefly, cultures were fixed with 4% paraformaldehyde (Electron Microscopy Tools) in DPBS (Life Technologies), washed with PBS, air dried, then blocked and permeabilized in 20% normal goat serum (NGS) (Sigma-Aldrich) plus 0.1% Triton X-100 (Sigma-Aldrich) in DPBS. The cultures were incubated in 20% NGS in dPBS plus primary antibodies. Cultures were washed in PBS, and incubated in 20% NGS in dPBS plus secondary antibodies. The cultures were washed in PBS then distilled water, air dried and then mounted on microscope slides with Fluorescence Mounting Medium (Dako).

Spinal cord tissue was collected from P30-33 mice using standard techniques. Briefly, after transcardial perfusion with PBS and then 4% paraformaldehyde (Electron Microscopy Tools), the spinal cord was dissected out and post-fixed in 4% paraformaldehyde overnight at 4° Celsius and cryoprotected by incubation in 30% sucrose in PBS until tissue sank. Coronal sections were cut in 30-micrometer thick slices from the cervical spinal cord (C5-C8) using a freezing microtome (Microm HM 450 and KS 34, Thermo Scientific). Sections were immunostained with the same methods as cell cultures above.

Images were collected using a Zeiss Axio Imager Z1 Apotome or M2 Apotome.2 fluorescence microscope with either Axiovision or Zen software (Zeiss). Images are shown as a maximum intensity projection of optical section z-stacks. Micropillar cultures (Mei et al., 2014) and semi-thin sections were imaged using a Zeiss LSM-700 confocal microscope and Zen software.

Antibodies

Antibodies used for immunostaining are: microtubule associated protein 2 (chicken anti-MAP2, 1:1,000, Chemicon AB5543); neurofilament (mouse anti-NF, 1:200, Covance SMI-312R); junction adhesion molecule 2 (rabbit anti-JAM2, 1:100-200, ThermoFisher Scientific PA5-21576); myelin basic protein (rat anti-MBP, 1:100, Millipore MAB386); p75-neurotrophin receptor (mouse anti-p75NTR, 1:25 hybridoma supernatant, MC192); contactin associated protein (mouse anti-CASPR, 1:500, E. Peles laboratory), neuronal nuclei (rabbit anti-NeuN, 1:2000 Abcam ab177487), adenomatous polyposis coli (mouse anti-APC/CC1, 1:200 Millipore OP80), beta-galactosidase (chicken anti-βGal, 1:1000 Aves Labs BGL-1040), vesicular glutamate transporter 2 (guinea pig anti-VGLUT2, 1:4,000 Millipore AB2251), vesicular glutamate transporter 1 (guinea pig anti-VGLUT1, 1:4,000), vesicular GABA transporter (guinea pig anti-VGAT, 1:500 Synaptic Systems 131 004), paired box gene 2 (rabbit anti-PAX2, 1:1,000-4,000 Abcam ab79389), and platelet derived growth factor receptor-alpha (rabbit anti-PDGFRα, 1:8,000, generous gift of W.B. Stallcup, Sanford-Burnham Medical Research Institute, Cancer Center, La Jolla, CA USA). Secondary antibodies were Alexa Fluor raised in goat against rat, mouse, rabbit, human or chicken in the following wavelengths: 488, 594, 647 (1:1,000 Life Technologies) and nuclei were stained with DAPI. The antibodies used in function-blocking experiments (Figure S1): rat anti-JAM2 (5μg/mL, R&D Systems MAB9881) or rat IgG (5μg/mL, R&D Systems 6-001-F).

Primary neuron and glia isolation and culture

Spinal cord neuron (SCN) isolation and culture has been described previously (Camu and Henderson, 1992; Molofsky et al., 2014). Briefly, embryonic day 15 rat or mouse embryo spinal cords were dissected and meninges removed as much as possible. Spinal cords were chopped with a sterile scalpel blade and the tissue was incubated in 0.05% trypsin-EDTA (Life Technologies) for 15 minutes at 37° Celsius. The tissue was dissociated into a single-cell suspension and incubated in a series of immunopanning dishes; two negative selection dishes coated with monoclonal hybridoma antibodes rat neural antigen-2 (Ran-2, ATCC) and Galactocerebrocide (Gal-C (Ranscht et al., 1982)); and one positive selection plate against p75 neurotrophin receptor (p75NTR, rat cells: MC192 hybridoma; mouse cells: rabbit anti-p75 function blocking antibody 'REX', a generous gift of L.F. Reichardt (Weskamp and Reichardt, 1991)). Adherent cells were released from the final immunopanning plate with a brief application of 0.05% trypsin-EDTA and 200,000-300,000 cells were seeded on 25mm round coverslips prepared with 200µL of 1:25 Matrigel (Corning, 356230) in DMEM (Life Technologies). SCN were left to adhere overnight, and flooded with growth medium plus 5-fluoro-2'-deoxyuridine (FDU) to kill mitotic cells, and 80% of growth medium was changed every three days for 3-4 weeks: DMEM (Life Technologies), B27 (Life Technologies), N2 (Life Technologies), penicillin-streptomycin (Life Technologies), N-acetylcisteine (NAC, Sigma-Aldrich), forskolin (EMD), insulin (Sigma-Aldrich), brain-derived neurotrophic factor (BDNF, Peprotech), ciliary neurotrophic factor (CNTF, Peprotech), glial-derived neurotrophic factor (GDNF, Peprotech).

Dorsal root ganglion (DRG) neuron cultures were established as previously described (Mei et al., 2014). Oligodendrocyte precursor cells (OPCs) were isolated (Lee et al., 2013) and cultured on micropillars as previously described (Mei et al., 2014).

OPCs were cocultured with 3-4 week old SCN as follows: OPCs were isolated with hybridoma anti-A2B5 or anti-O4-coated panning dishes, and 400,000 OPCs were seeded on each SCN culture in chemically-defined medium (Lee et al., 2013), which was changed every three days. For Jam2-Fc or Fc cocultures (Figure 5), 10 micrograms/mL protein was added to culture medium.

Oligodendrocyte nanofiber and microbead culture

Aligned polycaprolactone nanofibers were purchased in an 8-chamber slide format (Nanofiber Solutions cat 0802). 20 micrometer-diameter NH_2 polystyrene beads (Kisker Biotech Gmbh & Co cat PPS-20.0NH2) were sparsely seeded into the nanofiber chambers, coated with poly-L-lysine and dried to promote adhesion of beads to the nanofibers. OPC culture on beads and nanofibers was performed essentially as described (Chong et al., 2011; Lee et al., 2013). OPCs were seeded into the chambers and cultured for 3-4 days, then fixed and immunostained as above.

Oligodendrocyte coculture on live and cross-linked SCNs

SCN cultures were established as above. Prior to OPC seeding, SCN cultures were chemically cross-linked as described (Rosenberg et al., 2008) with 4% paraformaldehyde for 10 minutes at room temperature. Fixed neuron cultures were extensively washed in L15 medium + 10% FBS (Gibco), and

finally washed with coculture medium. One million OPCs were seeded onto either live or cross-linked neurons and cocultured for 5 days (Figure 2) or 7-12 days (Figure 1) in a chemically defined medium, then immunostained as above.

Micropillar protein coating

Micropillar arrays were sterilized with 100% ethanol and dried. Micropillars were coated with poly-L-lysine for one hour at room temperature, washed three times with water and dried. Each micropillar array of 1000 pillars was then coated with 2µg of either Fc protein (R&D Systems 110-HG) or JAM2-Fc protein (R&D Systems 988-VJ-050) in 27µL Tris HCl pH 9.5 overnight at room temperature. The micropillars were washed three times with water and twice with oligodendrocyte culture medium and kept wet with medium until 40,000 OPCs were seeded.

JAM2-Fc and Fc protein binding assay

OPCs were seeded onto poly-L-lysine coated coverslips in PDGF-containing culture medium overnight. On div 3, coverslips were washed with DMEM and incubated in 2µg/mL JAM2-Fc or Fc in DMEM for 30 minutes at room temperature. The coverslips were washed three times with DPBS, fixed with paraformaldehyde and immunostained as above.

Western Blot Analysis

Western blotting was performed essentially as previously described (Rosenberg et al., 2008). 25mm coverslips containing either SCN alone or myelinating SCN cocultures were collected in 100µL/coverslip of ice cold RIPA buffer, kept on ice and frozen immediately at -80$^{\circ C}$. Samples were thawed on ice and homogenized. Protein concentration was determined by BCA Protein Assay (Thermo Scientific 23225). Proteins were transferred to pure nitrocellulose membranes and probed with primary antibodies (see **Antibodies**) and Alexa Fluor 680 secondary antibodies raised in goat (Life Technologies). Imaging was conducted with an Odyssey infrared system (LI-COR).

RNA isolation, RNA sequencing and bioinformatics

Spinal cords and dorsal root ganglia were dissected from a single litter of embryonic-day 15 rat embryos, SCN and DRG neurons were isolated and cultured for three weeks as described above. RNA was isolated using Trizol Reagent and manufacturer's protocol (Life Technologies). Sequencing was performed with Illumina Genome Analyzer Sequencing System. Over 142M single end reads of length 100 bases were sequenced per sample. Sequences were produced with CASAVA (version 1.8.1.) and aligned to Rattus norvegicus rn4 genome build using TopHat (version 1.3.0) (Trapnell et al., 2009). TopHat was run separately for each RNA-Seq library with the options "--segment-mismatches 1 --min-intron-length 30 --max-multihits 10 --solexa-quals -o". Transcriptome was assembled using Cufflinks (Roberts et al., 2011; Trapnell et al., 2010) (version 1.1.0) and RefSeq reference annotation file (using the options –g).The reference was downloaded from the UCSC tables. The two assembled transcriptomes

were merged with the tool Cuffmerge (version 1.1.0.). Cuffdiff was used to detect differentially expressed genes and transcripts between the two samples. Identification of the rat transcripts coding for membrane and transmembrane proteins was done with Ingenuity® Pathway Analysis (IPA®). The criteria for selection of differentially expressed transcripts was a higher expression in SCNs as compared to DRGs expression, q values <=0.05 and p values <=0.05.

Quantitative PCR

Total RNA was extracted from three-week-old spinal cord neuron or dorsal root ganglion neuron cultures using Trizol Reagent (Life Technologies), and precipitated using either chloroform and isopropanol or PureLink RNA Mini Kit (Life Technologies, cat. 12183020). RNA was reverse transcribed using the RETROscript kit oligo-dT primers (Thermo Fisher, cat. AM1710). cDNA was amplified in triplicate using Power SYBR Green PCR master mix (Thermo Fisher, cat. 4367659) and primers for either *jam2* (Forward 5' TACTGTGAAGCCCGCAACTC 3', Reverse 5' GCAGAAATGACGAAGGCCAC 3', product length 122 base pairs), or *gapdh* (Forward 5' GTGCCAGCCTCGTCTCATAG 3', Reverse 5' AGAGAAGGCAGCCCTGGTAA 3', product length 91 base pairs). qPCR was run on a 7500 Real Time PCR system and analyzed with 7500 software version 2.0.6 (Applied Biosystems).

Electron microscopy

Transmission electron microscopy of cell cultures is as described previously (Lee et al., 2013; Rosenberg et al., 2008). Briefly, cultures were fixed with 4% PFA (Electron Microscopy Tools), incubated in 1% osmium tetroxide (Electron Microscopy Tools), then counterstained with 1% uranyl acetate. Samples were dehydrated in a series of ethanol dilutions and embedded in 1:1 EMBed-812 resin (Electron Microscopy Sciences) to propylene oxide (PPO, Electron Microscopy Sciences), then incubated in a 2:1 resin to PPO mixture. Cultures were detached from the coverslip with a razor blade and rolled tightly before embedding into the final 100% resin block. Ultrathin sections were cut at the W.M. Keck Foundation Advanced Microscopy Laboratory and imaged with a JEM1400 Electron Microscope (JEOL) in the Zilkha Neurogenetic Institute. Scanning electron microscopy of micropillars is as described previously (Mei et al., 2014).

Image analysis and statistics

The UCSF department of Biostatistics was consulted to identify suitable statistical tests. Statistical significance was determined at P-values < 0.05. Statistical tests were applied as described in figure legends. Data normality was determined using the Kolmogorov–Smirnov test. N values are indicated in the figure legends.

Author Contributions

S.A.R., F.M., Y.E.E., L.A.O., D.L., Y.A.S., J.N.K. and J.R.C. performed experiments. Y.E.E., M.A.L., E.P. and J.R.C. provided reagents. S.A.R., F.M., Y.E.E., L.A.O., Y.A.S., J.N.K., D.A.L., E.P. and J.R.C.

provided intellectual contributions. S.A.R., D.L. and J.R.C. analyzed the data. S.A.R. and J.R.C. wrote the paper.

Acknowledgements

We thank Dr. W.B. Stallcup and Dr. L.F. Reichardt for antibodies, M.L. Wong for ultrathin sectioning of electron microscopy samples, J. Wong for semi-thin sectioning and toluidine blue staining (Gladstone Institutes Electron Microscopy Core, San Francisco, CA). We also thank Dr. K.J. Chang for technical assistance, Dr. S.Y.C. Chong for efforts on development of SCN culture conditions, members of the Chan Laboratory for critical reading of the manuscript, and the UCSF Clinical and Translational Science Institute, for biostatistics consultation (NIH UL1 TR000004). This work was supported by NMSS Research Grants (RG4541A3 and RG5203A4), NIH/NINDS (R01NS062796, R01NS097428) and the Rachleff Family Professorship to J.R.C.; NIH/NINDS (R01NS50220), and the Dr. Miriam and Sheldon G. Adelson Medical Research Foundation, the Incumbent of the Hanna Hertz Professorial Chair for Multiple Sclerosis and Neuroscience to E.P.; NSERC PGS D to L.A.O.; and NIH/NINDS Ruth L. Kirschstein NRSA (F31NS081905) to S.A.R.

References

Arcangeli, M.-L., Frontera, V., Bardin, F., Obrados, E., Adams, S., Chabannon, C., Schiff, C., Mancini, S.J.C., Adams, R.H., and Aurrand-Lions, M. (2011). JAM-B regulates maintenance of hematopoietic stem cells in the bone marrow. Blood *118*, 4609–4619.

Arcangeli, M.-L., Frontera, V., and Aurrand-Lions, M. (2013). Function of junctional adhesion molecules (JAMs) in leukocyte migration and homeostasis. Arch. Immunol. Ther. Exp. (Warsz.) *61*, 15–23.

Bechler, M.E., Byrne, L., and Ffrench-Constant, C. (2015). CNS Myelin Sheath Lengths Are an Intrinsic Property of Oligodendrocytes. Curr. Biol. CB *25*, 2411–2416.

Blinzinger, K., Anzil, A.P., and Müller, W. (1972). Myelinated nerve cell perikaryon in mouse spinal cord. Z. Für Zellforsch. Mikrosk. Anat. Vienna Austria 1948 *128*, 135–138.

Braak, E., Braak, H., and Strenge, H. (1977). The fine structure of myelinated nerve cell bodies in the bulbus olfactorius of man. Cell Tissue Res. *182*, 221–233.

Camu, W., and Henderson, C.E. (1992). Purification of embryonic rat motoneurons by panning on a monoclonal antibody to the low-affinity NGF receptor. J. Neurosci. Methods *44*, 59–70.

Chang, A., Tourtellotte, W.W., Rudick, R., and Trapp, B.D. (2002). Premyelinating oligodendrocytes in chronic lesions of multiple sclerosis. N. Engl. J. Med. *346*, 165–173.

Chong, S.Y.C., Rosenberg, S.S., Fancy, S.P.J., Zhao, C., Shen, Y.-A.A., Hahn, A.T., McGee, A.W., Xu, X., Zheng, B., Zhang, L.I., et al. (2011). Neurite outgrowth inhibitor Nogo-A establishes spatial segregation and extent of oligodendrocyte myelination. Proc. Natl. Acad. Sci. *109*, 1299–1304.

Cooper, M.H., and Beal, J.A. (1977). Myelinated granule cell bodies in the cerebellum of the monkey (Saimiri sciureus). Anat. Rec. *187*, 249–255.

Einheber, S., Zanazzi, G., Ching, W., Scherer, S., Milner, T.A., Peles, E., and Salzer, J.L. (1997). The axonal membrane protein Caspr, a homologue of neurexin IV, is a component of the septate-like paranodal junctions that assemble during myelination. J. Cell Biol. *139*, 1495–1506.

Eisenbach, M., Kartvelishvily, E., Eshed-Eisenbach, Y., Watkins, T., Sorensen, A., Thomson, C., Ranscht, B., Barnett, S.C., Brophy, P., and Peles, E. (2009). Differential clustering of Caspr by oligodendrocytes and Schwann cells. J. Neurosci. Res. *87*, 3492–3501.

Fancy, S.P.J., Harrington, E.P., Yuen, T.J., Silbereis, J.C., Zhao, C., Baranzini, S.E., Bruce, C.C., Otero, J.J., Huang, E.J., Nusse, R., et al. (2011). Axin2 as regulatory and therapeutic target in newborn brain injury and remyelination. Nat. Neurosci. *14*, 1009–1016.

Franklin, R.J.M., and ffrench-Constant, C. (2008). Remyelination in the CNS: from biology to therapy. Nat. Rev. Neurosci. *9*, 839–855.

Gibson, E.M. (2014). Neuronal activity promotes oligodendrogenesis and adaptive myelination in the mammalian brain. Science *344*, 1252304.

Hines, J.H., Ravanelli, A.M., Schwindt, R., Scott, E.K., and Appel, B. (2015). Neuronal activity biases axon selection for myelination in vivo. Nat Neurosci *18*, 683–689.

Lee, S., Leach, M.K., Redmond, S.A., Chong, S.Y.C., Mellon, S.H., Tuck, S.J., Feng, Z.-Q., Corey, J.M., and Chan, J.R. (2012). A culture system to study oligodendrocyte myelination processes using engineered nanofibers. Nat Meth *9*, 917–922.

Lee, S., Chong, S.Y.C., Tuck, S.J., Corey, J.M., and Chan, J.R. (2013). A rapid and reproducible assay for modeling myelination by oligodendrocytes using engineered nanofibers. Nat. Protoc. *8*, 771–782.

Lee, X., Yang, Z., Shao, Z., Rosenberg, S.S., Levesque, M., Pepinsky, R.B., Qiu, M., Miller, R.H., Chan, J.R., and Mi, S. (2007). NGF regulates the expression of axonal LINGO-1 to inhibit oligodendrocyte differentiation and myelination. J. Neurosci. Off. J. Soc. Neurosci. *27*, 220–225.

Lubetzki, C., Demerens, C., Anglade, P., Villarroya, H., Frankfurter, A., Lee, V.M., and Zalc, B. (1993). Even in culture, oligodendrocytes myelinate solely axons. Proc. Natl. Acad. Sci. U. S. A. *90*, 6820–6824.

Mei, F., Fancy, S.P.J., Shen, Y.-A.A., Niu, J., Zhao, C., Presley, B., Miao, E., Lee, S., Mayoral, S.R., Redmond, S.A., et al. (2014). Micropillar arrays as a high-throughput screening platform for therapeutics in multiple sclerosis. Nat Med *20*, 954–960.

Mensch, S., Baraban, M., Almeida, R., Czopka, T., Ausborn, J., El Manira, A., and Lyons, D.A. (2015). Synaptic vesicle release regulates myelin sheath number of individual oligodendrocytes in vivo. Nat Neurosci *18*, 628–630.

Mi, S., Miller, R.H., Lee, X., Scott, M.L., Shulag-Morskaya, S., Shao, Z., Chang, J., Thill, G., Levesque, M., Zhang, M., et al. (2005). LINGO-1 negatively regulates myelination by oligodendrocytes. Nat Neurosci *8*, 745–751.

Molofsky, A.V., Kelley, K.W., Tsai, H.-H., Redmond, S.A., Chang, S.M., Madireddy, L., Chan, J.R., Baranzini, S.E., Ullian, E.M., and Rowitch, D.H. (2014). Astrocyte-encoded positional cues maintain sensorimotor circuit integrity. Nature *509*, 189–194.

Pedraza, L., Huang, J.K., and Colman, D. (2009). Disposition of axonal caspr with respect to glial cell membranes: Implications for the process of myelination. J. Neurosci. Res. *87*, 3480–3491.

Ranscht, B., Clapshaw, P.A., Price, J., Noble, M., and Seifert, W. (1982). Development of oligodendrocytes and Schwann cells studied with a monoclonal antibody against galactocerebroside. Proc. Natl. Acad. Sci. U. S. A. *79*, 2709–2713.

Remahl, S., and Hildebrand, C. (1985). Myelinated non-axonal neuronal elements in the feline olfactory bulb lack sites with a nodal structural differentiation. Brain Res. *325*, 1–11.

Roberts, A., Pimentel, H., Trapnell, C., and Pachter, L. (2011). Identification of novel transcripts in annotated genomes using RNA-Seq. Bioinforma. Oxf. Engl. *27*, 2325–2329.

Rosenberg, S.S., Kelland, E.E., Tokar, E., De la Torre, A.R., and Chan, J.R. (2008). The geometric and spatial constraints of the microenvironment induce oligodendrocyte differentiation. Proc. Natl. Acad. Sci. U. S. A. *105*, 14662–14667.

Ruckh, J.M., Zhao, J.-W., Shadrach, J.L., van Wijngaarden, P., Rao, T.N., Wagers, A.J., and Franklin, R.J.M. (2012). Rejuvenation of Regeneration in the Aging Central Nervous System. Cell Stem Cell *10*, 96–103.

Sharma, K., Schmitt, S., Bergner, C.G., Tyanova, S., Kannaiyan, N., Manrique-Hoyos, N., Kongi, K., Cantuti, L., Hanisch, U.-K., Philips, M.-A., et al. (2015). Cell type- and brain region-resolved mouse brain proteome. Nat. Neurosci. *18*, 1819–1831.

Smith, K.M., Boyle, K.A., Madden, J.F., Dickinson, S.A., Jobling, P., Callister, R.J., Hughes, D.I., and Graham, B.A. (2015). Functional heterogeneity of calretinin-expressing neurons in the mouse superficial dorsal horn: implications for spinal pain processing. J. Physiol. *593*, 4319–4339.

Trapnell, C., Pachter, L., and Salzberg, S.L. (2009). TopHat: discovering splice junctions with RNA-Seq. Bioinforma. Oxf. Engl. *25*, 1105–1111.

Trapnell, C., Williams, B.A., Pertea, G., Mortazavi, A., Kwan, G., van Baren, M.J., Salzberg, S.L., Wold, B.J., and Pachter, L. (2010). Transcript assembly and quantification by RNA-Seq reveals unannotated transcripts and isoform switching during cell differentiation. Nat. Biotechnol. *28*, 511–515.

Trapp, B.D., and Nave, K.-A. (2008). Multiple sclerosis: an immune or neurodegenerative disorder? Annu. Rev. Neurosci. *31*, 247–269.

Weskamp, G., and Reichardt, L.F. (1991). Evidence that biological activity of NGF is mediated through a novel subclass of high affinity receptors. Neuron *6*, 649–663.

Yuen, T.J., Silbereis, J.C., Griveau, A., Chang, S.M., Daneman, R., Fancy, S.P.J., Zahed, H., Maltepe, E., and Rowitch, D.H. (2014). Oligodendrocyte-encoded HIF function couples postnatal myelination and white matter angiogenesis. Cell *158*, 383–396.

Zalc, B., Goujet, D., and Colman, D. (2008). The origin of the myelination program in vertebrates. Curr. Biol. CB *18*, R511–R512.

Figure Legends

Figure 1. Myelin target selection by oligodendroglia. (**a**) Models of oligodendrocyte axon selection and myelination. Attraction: an attractive cue is expressed on the axon (green), resulting in its myelination by the oligodendrocyte, while no myelination cues are present on non-myelinated structures (gray). Inhibition: non-myelinated structures express an inhibitory cue (red), resulting in oligodendrocyte process inhibition and myelination of inhibition-free axons (gray). Mixed: Inhibitory (red) and attractive (green) cues result in the correct myelination of axons. (**b**) a phase image of a spinal cord neuron (SCN) in culture. (**c**) a phase image of nanofibers and a 20-micrometer diameter polystyrene bead. (**d**) an oligodendrocyte ensheathing myelin basic protein-positive (MBP+, red) membranes on nanofibers and the bead shown in (**c**) with a side-view shown in the inset. (**e**) a neuron at eight days in vitro immunostained for microtubule associated protein 2 (MAP2) and neurofilament (NF). (**f**) electron micrograph of a synapse, and (**g**) neurofilament-positive axons in SCN cultures. (**h**) low-magnification image of neurons and oligodendroglia in a myelinating coculture. (**i**) timecourse of oligodendrocyte progenitor cell (OPC) and oligodendrocyte protein expression in SCN myelinating cocultures. (**j**) electron micrograph of a myelinated axon in a myelinating spinal cord neuron coculture. Scale bars = 20 micrometers (**d**), 10 micrometers (**e**), 250 nanometers (**f**), 500 nanometers (**g, i**), 50 micrometers (**h**).

Figure 2. Oligodendrocytes wrap somatodendritic compartments of chemically cross-linked neurons. (**a**) an oligodendrocyte (asterisk) forms MBP+ myelin segments on SCN axons (NF, white) but not dendrites (MAP2, green). (**b**) an oligodendrocyte (asterisk) forms myelin segments on paraformaldehyde cross-linked SCN axons, dendrites (arrowheads), and somata (arrows). (**c**) quantification of MBP+ ensheathments on either MAP2+ dendrites or NF+ axons in live and cross-linked ('Fixed') cocultures. (**d**-**e**) multiple layers of myelin membrane formed in a cross-linked myelinating coculture. DAPI, blue. Bar graph in (**c**) represents means with s.e.m. error bars. n = 4 experiments quantified from 26-30 20x fields per condition per experiment. Significance was calculated using one-tailed paired Students t-test. P = 0.04. Scale bars = 20 micrometers (**a**,**b**), 500 nanometers (**d**), 100 nanometers (**e**).

Figure 3. Differential RNA-Seq and candidate profiling. (**a**) Experimental procedure for RNA extraction. Embryonic day 15 (E15) rat embryos were dissected and their spinal cords and dorsal root ganglia were isolated. SCN and dorsal root ganglion neurons (DRG) were separately cultured and their RNA was collected for sequencing (RNA-seq). (**b**) Results of differential RNA-seq. Candidate inhibitory proteins are SCN transcripts that are significantly differentially expressed (large pie chart, right), are localized to the plasma membrane and have transmembrane domains (pink). Transcripts detected also included other SCN transcripts (big pie chart, light gray), SCN enriched, but not significantly differentially expressed (small pie chart, gray), DRG-enriched transcripts (black) and not differentially expressed transcripts

(n.d.e.). (**c**) Volcano plot of DRG (black) and SCN (dark gray), SCN candidate ("Candidate", pink), and not significantly differentially expressed ("n.s.", light gray) transcripts. (**d**) Examples of differentially expressed transcripts from (**c**). (**e**) qPCR amplification of *jam2* from cultured DRG and SCN, normalized to DRG expression. (**f**) DRG somata and axons (P75, green) immunostained for JAM2 (red), and (**g**) Cultured SCN somatodendritic compartment (MAP2, green) and axons (NF, white), and DAPI, blue. Bar graph in (**e**) represents mean and s.e.m. from n = 4 biological replicates. *Gapdh* was used as an internal control. Scale bars = 20 micrometers.

Figure 4. JAM2 is sufficient to inhibit oligodendrocyte wrapping. (**a**) JAM2-Fc or (**b**) Fc protein (white) was cultured with MBP+ oligodendrocytes (red) and PDGFRα+ OPCs (green) to demonstrate JAM2-Fc binding. (**c**) scanning electron micrograph micropillar array platform (left column) and immunostaining of a cultured oligodendrocyte wrapping a micropillar (MBP, right column) from the x-z plane/side view (top row) and x-y plane/top-down view (bottom row). (**d**) experimental setup: oligodendroglia are cultured on coated micropillars (left). Myelin membrane (red) wraps of differentiated oligodendrocytes are visualized as rings by taking an optical section (dashed gray box) through immunostained cultures (red ring in x-y plane, far right). Optical sections of (**e**) Fc- and (**f**) JAM2-Fc-coated micropillars immunostained for oligodendrocyte (MBP, red) and OPC (PDGFRα, green) wrapping, and micropillars (Fc protein, white). (**g**) The percentage of micropillars with a MBP+ or (**h**) PDGFRα+ ring, and the (**i**) densities of oligodendoglia on flat areas adjacent to micropillars. Box plots (**g**,**h**) are defined by the center median line, 25^{th} and 75^{th} percentiles determined by R software, whiskers extend 1.5 times the interquartile range from the 25^{th} and 75^{th} percentiles, and dots outside of whiskers are defined as outliers. n = 20 fields of 100 micropillars (dots) each condition pooled from four independent experiments. Significance was calculated using Wilcoxon Rank-Sum test. (**g**) *******, $P = 6.3x10^{-8}$; (**h**) ***, $P = 3.75x10^{-4}$. Bar graphs in (**i**) represent means with s.e.m. error bars. n = 18 10x fields (dots) each condition pooled from three independent experiments. Significance was calculated using two-tailed Students t-test. Scale bars: (**a**-**c**) 10 micrometers, (**e**-**f**) 400 micrometers.

Figure 5. JAM2 is sufficient to reduce myelin segment formation and is necessary to prevent somatodendritic wrapping *in vitro*. Oligodendrocytes in SCN cocultures form myelin segments in the presence of soluble (**a**) Fc or (**b**) JAM2-Fc protein. (**c**) the relative number of MBP+ segments formed in the presence of Fc or JAM2-Fc. (**d**) wildtype or (**e**) JAM2 KO neurons cocultured with wildtype OPCs for seven days *in vitro*. Arrowheads indicate myelin membranes on neuron soma and asterisks mark oligodendrocyte cell bodies. (**f**) the percentage of myelin membrane structures colocalized with MAP2+ and NF- somatodendritic compartments. (**g**) the percentage of neuron somata wrapped with MBP+ myelin membranes. (**h**) a wildtype MBP+ oligodendrocyte (asterisk) wraps membranes on a JAM2 KO MAP2+ neuron *in vitro*, clustering neuronal CASPR proteins (green). Bar graphs represent means with s.e.m. error bars. (**c**) n = 4 independent experiments (dots) representing median number of MBP+ segments

formed per oligodendrocyte from 59-79 oligodendrocytes quantified per experiment per condition. (**f**-**g**) n = 9 coverslips (dots) pooled from three independent experiments. Significance was calculated using one-tailed paired (**c**) or unpaired (**f**-**g**) Students t-test. (**c**) *, P = 0.032; (**f**) ****, P = 7.1×10^{-5}; (**g**) **, P = 0.0012. DAPI, blue. Scale bars: 20 micrometers.

Figure 6. JAM2 is necessary to inhibit somatic wrapping *in vivo*. (**a**) dorsal horn (dotted yellow line) in a coronal section of a wildtype spinal cord immunostained for MBP. (**b**) higher magnification of dorsal horn myelin (top, red), neurons (middle, green), and merged (bottom). (**c**-**d**) same as (**a**-**b**) but in JAM2 KO mice. Arrowheads indicate MBP+ wrapped MAP2+ neurons. (**e**) number of myelin wrapped dorsal horn neurons per hemisection (one dot = one hemisection, colors indicate littermate pairs). (**f**) bar graph of median number of wrapped neurons per hemisection per mouse. Connected diamonds indicate littermate pairs, and fill color corresponds to dots in (**e**). n = 5 littermate pairs, median taken from ten hemisections per mouse. *, P = 0.034; Wilcoxon Paired Signed-Ranks test. (**g**) a myelin wrapped neuron from a JAM2 KO dorsal horn imaged through an 11 micrometer thick z-stack. Individual columns labeled by z-plane depth, and a maximum intensity projection is shown in the far-right column. (**h**) a toluidine blue stained semi-thin section from a JAM2 KO mouse dorsal horn shows a myelin-wrapped neuron (pseudo-colored green cytoplasm and blue nucleus). Scale bars: (**a**-**d**) 50 micrometers, (**g**-**h**) 10 micrometers. DAPI, blue.

Figure 7. Pax2+ neurons are wrapped in JAM2 knockout mice. (**a**) dorsal horn immunostained for MBP, (**b**) Pax2, (**c**) label a subset of wrapped (**d**) MAP2+ neurons. (**e**) quantification of the percent of MBP+ 'bubbles' on Pax2+ neurons. (**f**) quantification of the percent of Pax2+ neurons wrapped by MBP+ 'bubbles'. (**g**) number of Pax2+ neurons per square millimeter in Jam2 +/- and Jam2-/- littermate pairs. n = 4 littermate pairs. Bar graphs represent: (**e**-**f**) median calculated as (**e**) total wrapped Pax2+ out of total wrapped cells per mouse, or (**f**) percent per field from 10 20x fields per mouse. Error bars represent median absolute deviation; (**g**) mean density per mouse calculated from 10 20x fields per mouse. Error bars represent s.e.m. *, P = 0.034; Wilcoxon Paired Signed-Ranks test. Scale bar: 50 micrometers.

Figure 8. Model of JAM2 function on oligodendrocyte wrapping. (**a**) a pre-myelinating process of an oligodendrocyte comes into contact with the somatodendritic compartment of a neuron. (**b**) in wildtype mice, somatodendritic JAM2 inhibits the oligodendrocyte process from wrapping. (**c**) when JAM2 is absent or blocked, the oligodendrocyte process is not inhibited, and continues to wrap myelin membranes on the neuron cell body.

Supplemental Figure 1. JAM2 function is necessary to prevent dendritic wrapping *in vitro*. (**a**) 7div myelinating SCN cultures incubated for the final two days with either IgG or (**b**) anti-JAM2 function blocking antibody. Oligodendrocytes (asterisks) wrap myelin membranes on axons (arrowheads) and on

dendrites (arrows). (**c**) the percentage of MBP+ myelin segments on MAP2+/NF- dendrites. Bar graphs represent means with s.e.m. error bars. Significance was calculated using one-tailed Students t-test. **, P = 0.0072. Scale bar: 10 micrometers.

Supplemental Figure 2. Oligodendrocyte ensheathment of JAM2 KO neurons *in vitro* and *in vivo* clusters somatodendritic CASPR protein. (**a**) a myelinating SCN coculture immunostained for MBP (red), CASPR (green) and MAP2 (white). Insets demonstrate examples of (**a1**) clustered CASPR on a wrapped neuron cell body, (**a2**) clustered CASPR on a wrapped dendrite, and (**a3**) no clustered CASPR signal on an unwrapped MAP2+ neuron. (**b**) a MAP2+ JAM2 KO dorsal horn neuron is wrapped *in vivo* by an MBP+ oligodendrocyte. At the edges of the MBP+ membrane is a spiraling line of clustered CASPR protein on the neuron surface. (**c**-**e**) a myelin-wrapped dorsal horn JAM2 KO neuron in three adjacent semi-thin sections stained with toluidine blue. The neuron cytoplasm is pseudo-colored green, and its nucleus is pseudo-colored blue. DAPI, blue. Scale bars: (**a-c**) 10 micrometers.

Supplemental Figure 3. JAM2 is widely expressed in spinal cord gray matter. Low-field images of the (**a**) dorsal and (**b**) ventral horns in a heterozygous *jam2:beta-galactosidase* knock-in reporter mouse shows widespread colocalization of NeuN+ beta-galactosidase+ cells. The ventral horns of (**c**) *jam2* heterozygous and (**d**) knockout mice show the presence of JAM2 protein on large neurons in MAP2+ gray matter. DAPI, blue. Scale bars: 50 micrometers.

Supplemental Figure 4. The spinal cord dorsal horn develops normally in JAM2 KO mice. Cross-sections of (**a**) JAM2 heterozygous (JAM2 Het) and (**b**) JAM2 KO show specific antibody labeling of JAM2 (white) on MAP2+ neuron cell bodies (arrowheads) in dorsal horn gray matter. In the dorsal horns of (**c**) WT and (**d**) JAM2 KO mice the densities of NeuN+ neurons and CC1+ oligodendrocytes is not significantly different. Quantification of (**e**) NeuN+ and (**f**) CC1+ cells in WT and JAM2 KO mouse dorsal horns. Bar graphs represent means with s.e.m. error bars. n = 3 littermate pairs. Significance was calculated using the paired two-tailed Students t-test. DAPI, blue. Scale bars: 20 micrometers.

Supplemental Figure 5. Pax2+ dorsal horn neurons have no or few somatic synapses *in vivo.* Quantification of the number of (**a**) VGLUT1, VGLUT2 or VGAT synapses onto PAX2+ neuronal somata in Jam2 -/- or Jam2 +/- mice. (**b**) VGAT puncta on a Pax2+ neuron soma. (**c**) a Pax2+ neuron wrapped by MBP+ membrane has no VGLUT1+ synaptic puncta on its soma. Bar graphs represent mean with s.e.m. error bars. n = 4 littermate pairs. Significance was calculated using the two-tailed Mann-Whitney U test. Scale bars: (**b**-**c**) 10 micrometers.

Figure 1

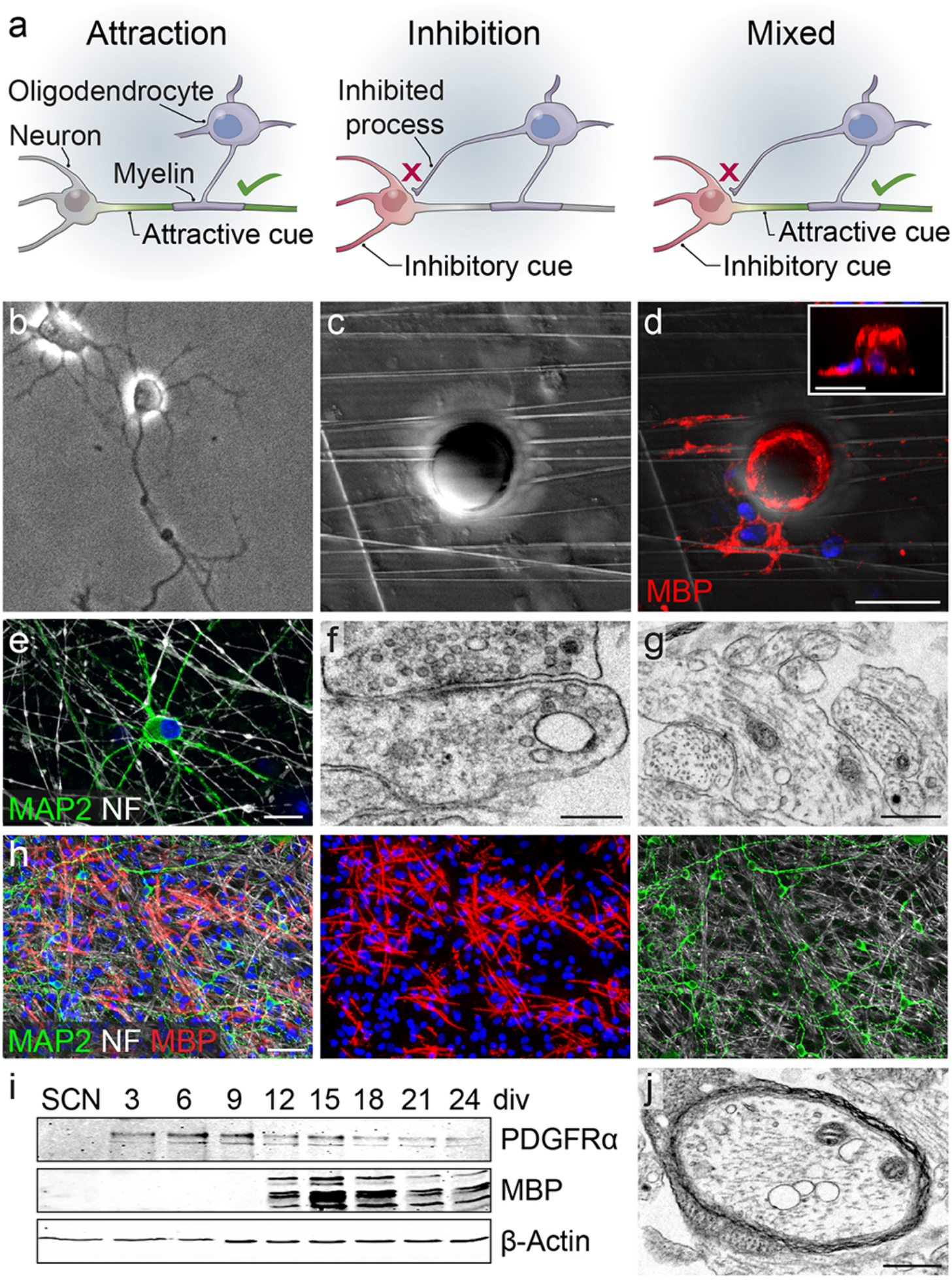
a
Attraction
Inhibition
Mixed
Oligodendrocyte
Neuron
Myelin
Attractive cue
Inhibited process
Inhibitory cue
Attractive cue
Inhibitory cue
b
c
d
MBP
e
MAP2 NF
f
g
h
MAP2 NF MBP
i
SCN 3 6 9 12 15 18 21 24 div
PDGFRα
MBP
β-Actin
j

Figure 2

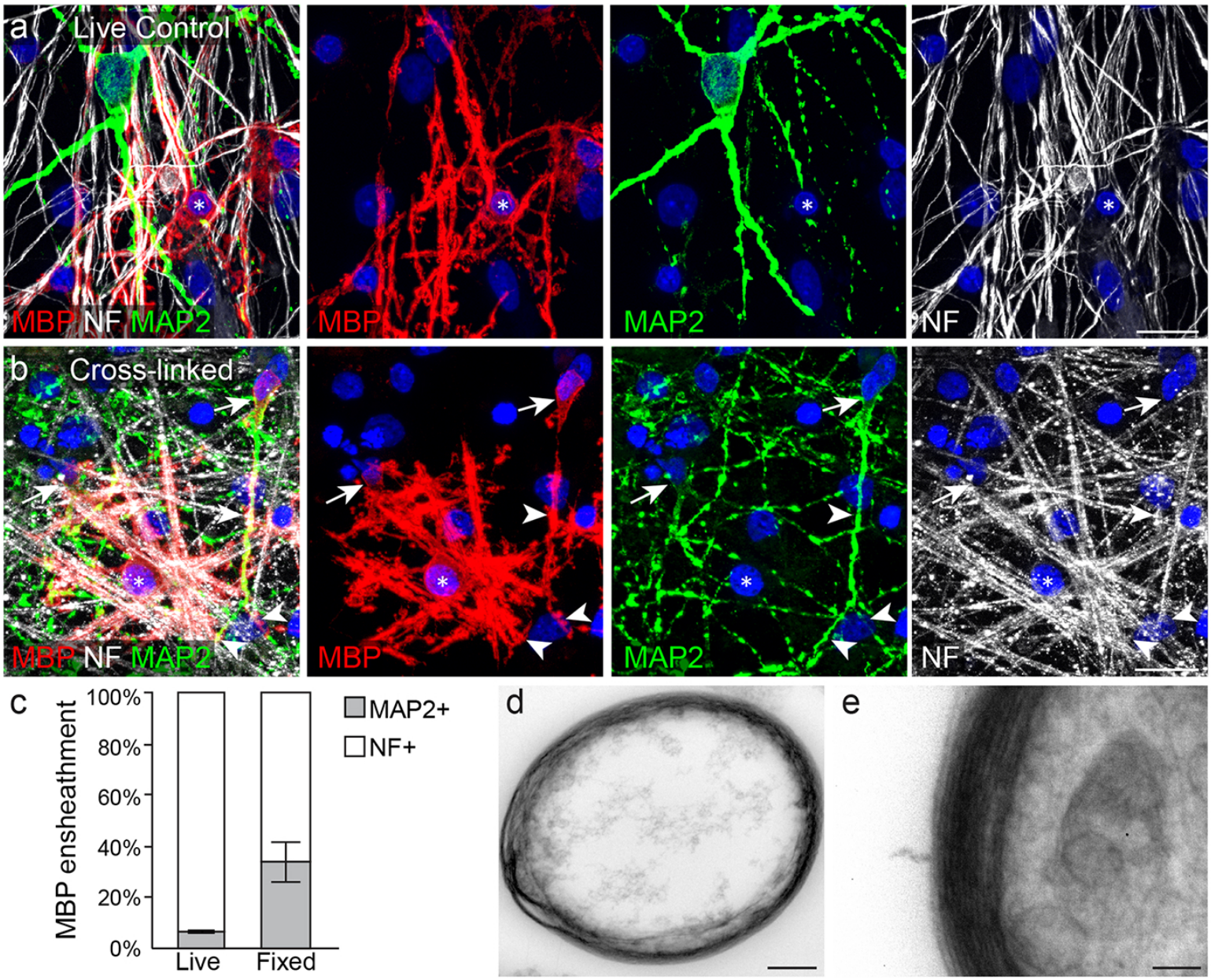
a
Live Control
MBP NF MAP2
MBP
MAP2
NF
b
Cross-linked
MBP NF MAP2
MBP
MAP2
NF
c
MBP ensheathment
100%
80%
60%
40%
20%
0%
Live
Fixed
MAP2+
NF+
d
e

Figure 3

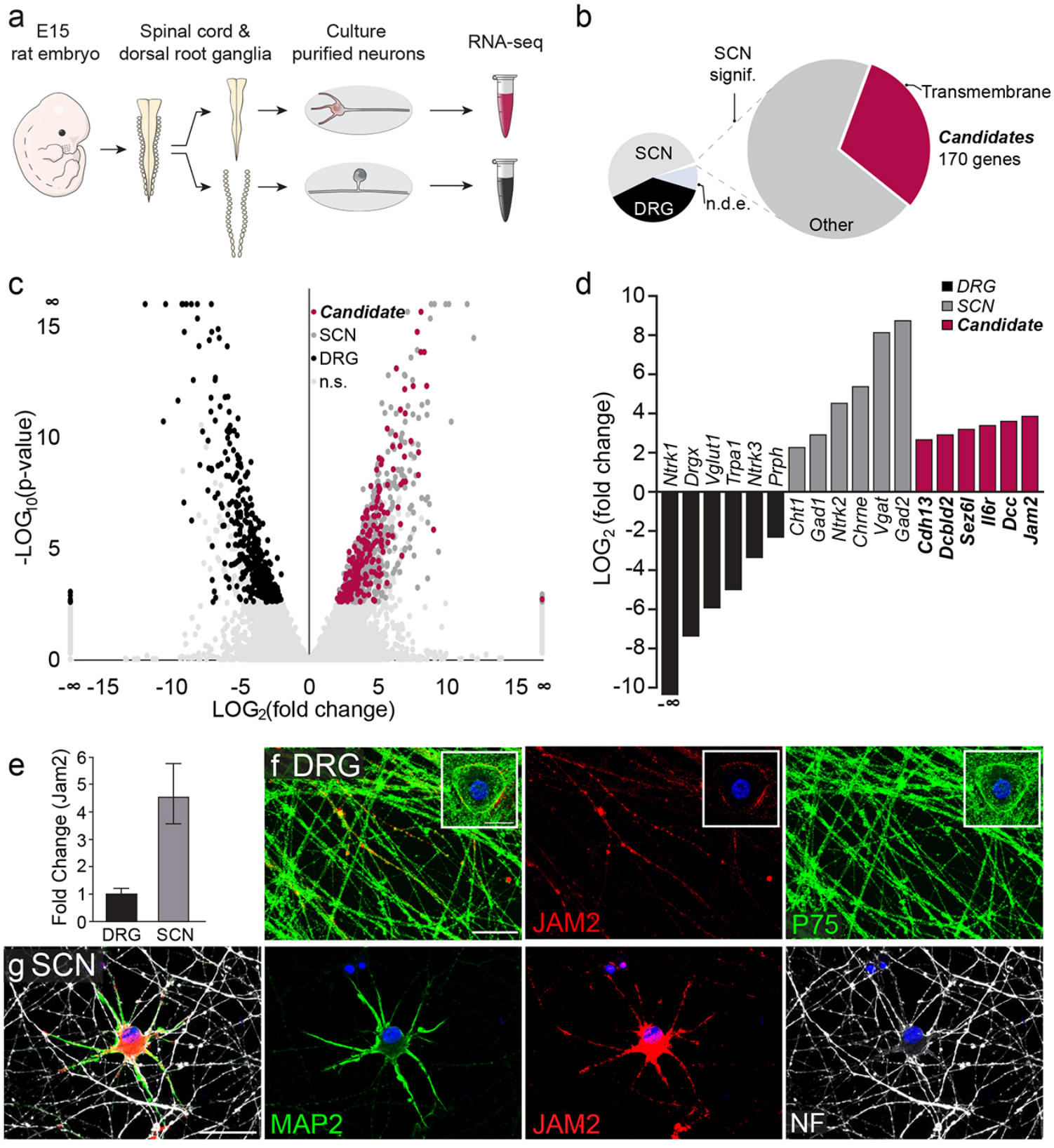
a
E15
rat embryo
Spinal cord &
dorsal root ganglia
Culture
purified neurons
RNA-seq
b
SCN
signif.
Transmembrane
Candidates
170 genes
SCN
DRG
n.d.e.
Other
c
Candidate
SCN
DRG
n.s.
-LOG10(p-value)
LOG2(fold change)
d
DRG
SCN
Candidate
LOG2 (fold change)
Ntrk1
Drgx
Vglut1
Trpa1
Ntrk3
Prph
Cht1
Gad1
Ntrk2
Chrne
Vgat
Gad2
Cdh13
Dcbld2
Sez6l
Il6r
Dcc
Jam2
e
Fold Change (Jam2)
DRG
SCN
f DRG
JAM2
P75
g SCN
MAP2
JAM2
NF

Figure 4

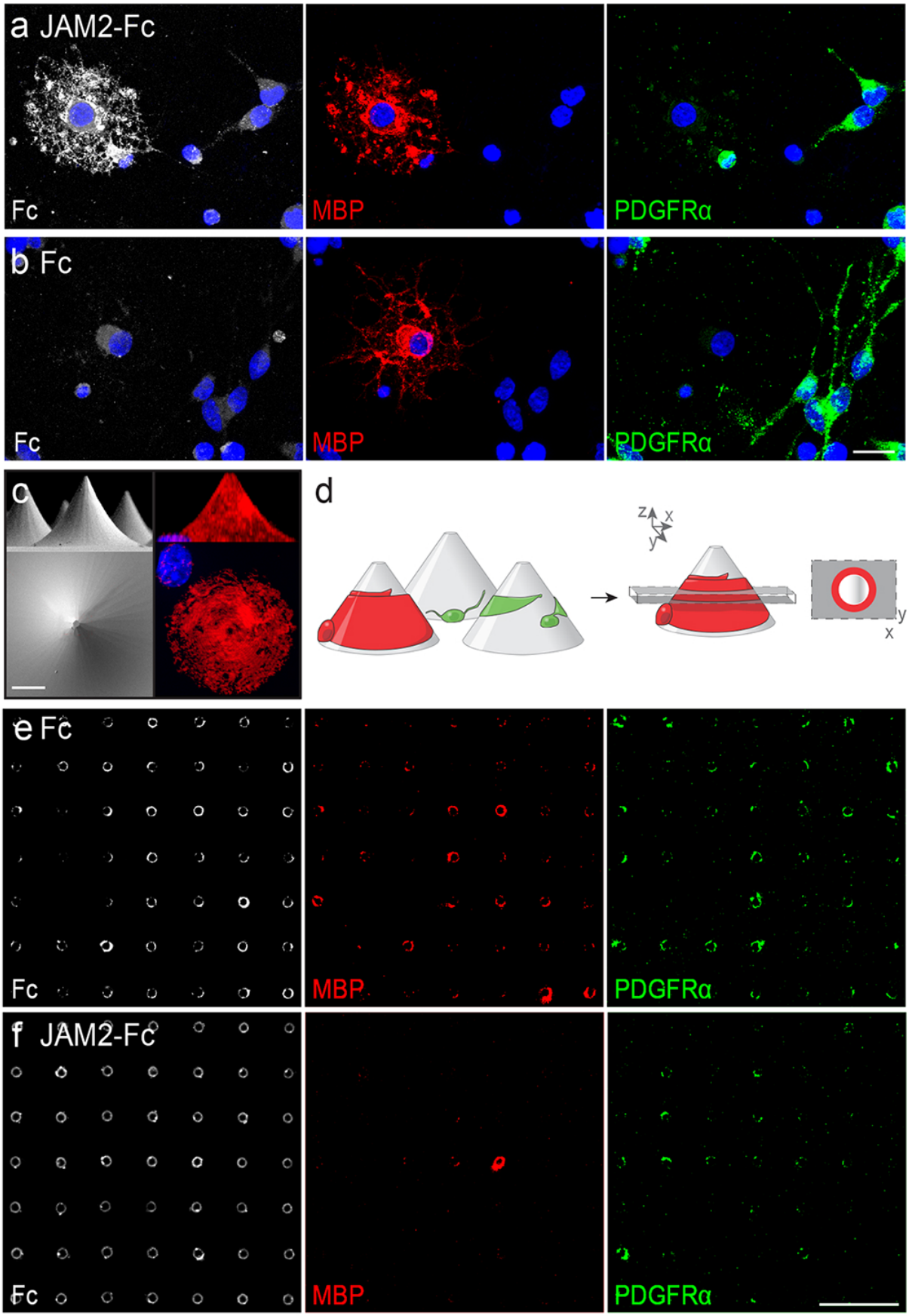
a JAM2-Fc
Fc
MBP
PDGFRα
b Fc
Fc
MBP
PDGFRα
c
d
z
x
y
y
x
e Fc
Fc
MBP
PDGFRα
f JAM2-Fc
Fc
MBP
PDGFRα

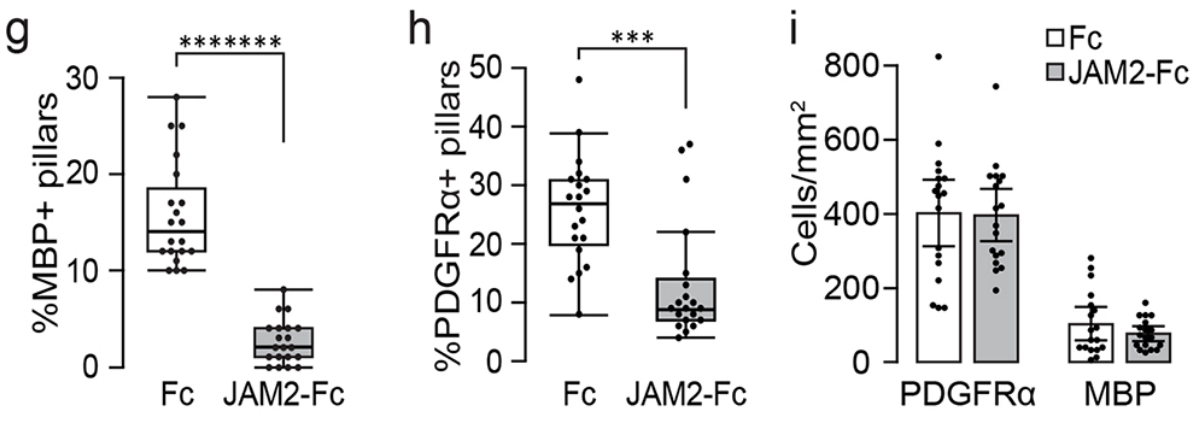
g
****
%MBP+ pillars
30
20
10
0
Fc
JAM2-Fc
h
***
%PDGFRα+ pillars
50
40
30
20
10
0
Fc
JAM2-Fc
i
Fc
JAM2-Fc
Cells/mm²
800
600
400
200
0
PDGFRα
MBP

Figure 5

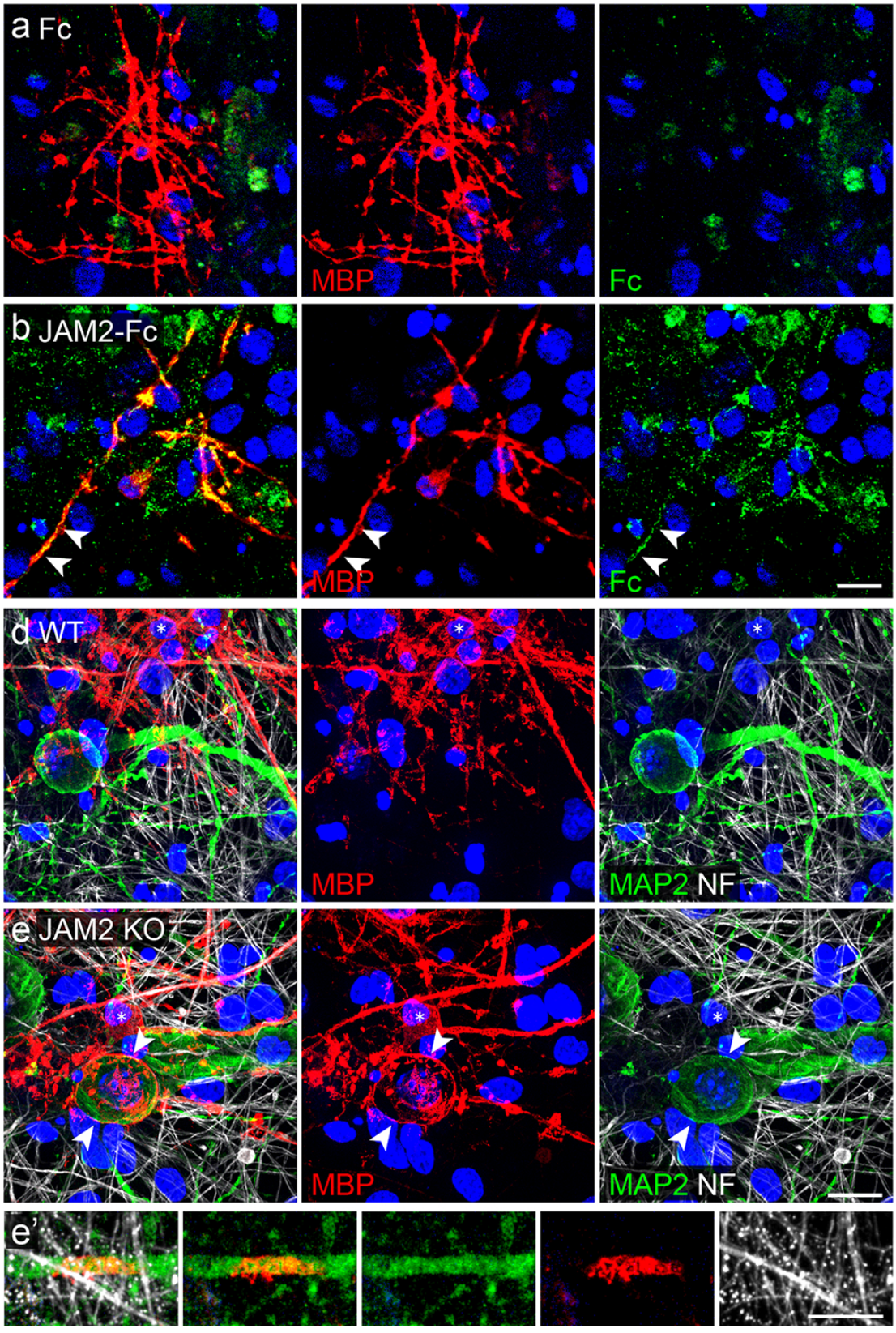
a Fc
MBP
Fc
b JAM2-Fc
MBP
Fc
d WT
MBP
MAP2 NF
e JAM2 KO
MBP
MAP2 NF
e'

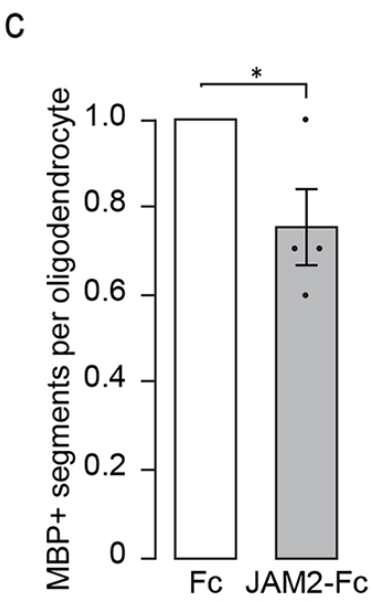
c
*
MBP+ segments per oligodendrocyte
1.0
0.8
0.6
0.4
0.2
0
Fc
JAM2-Fc

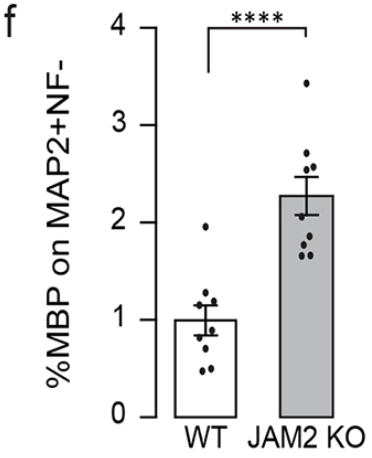
f
****
%MBP on MAP2+NF-
4
3
2
1
0
WT
JAM2 KO

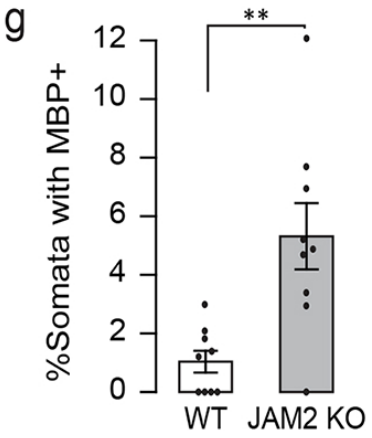
g
**
%Somata with MBP+
12
10
8
6
4
2
0
WT
JAM2 KO

Figure 6

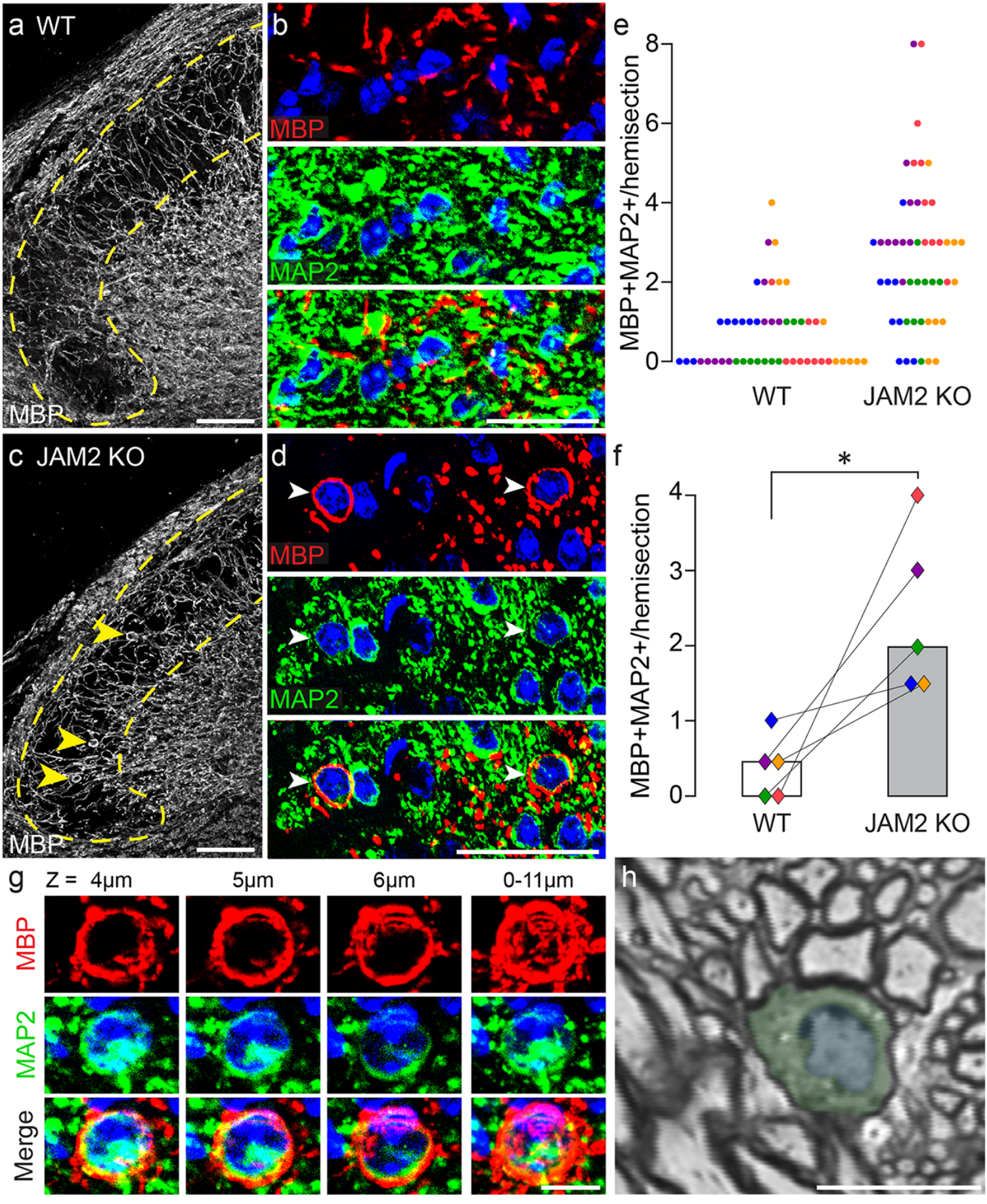
a WT
MBP
b
MBP
MAP2
c JAM2 KO
MBP
d
MBP
MAP2
e
MBP+MAP2+/hemisection
0
2
4
6
8
WT
JAM2 KO
f
*
MBP+MAP2+/hemisection
0
1
2
3
4
WT
JAM2 KO
g
Z = 4µm
5µm
6µm
0-11µm
MBP
MAP2
Merge
h

Figure 7

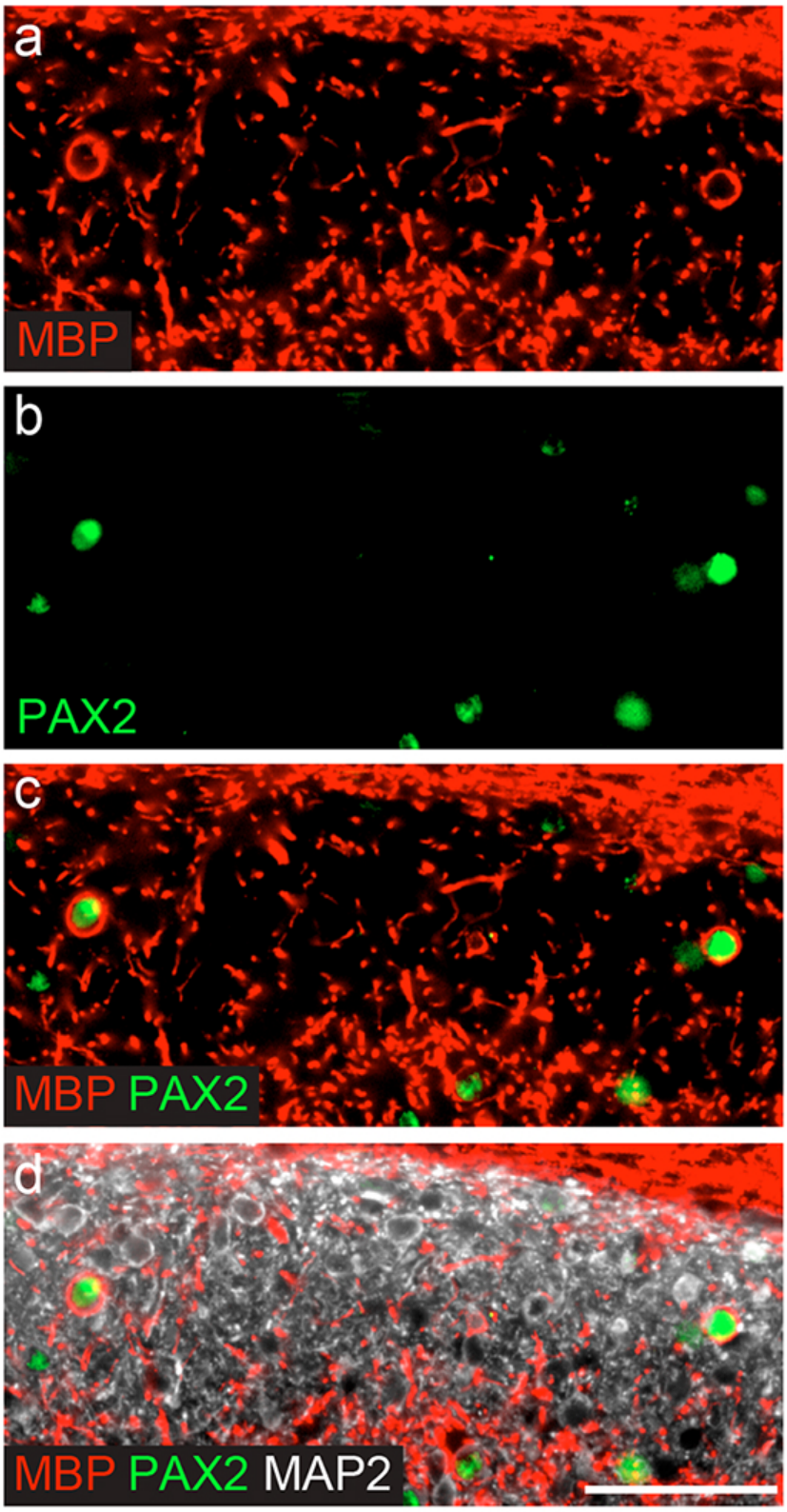
a
MBP
b
PAX2
c
MBP PAX2
d
MBP PAX2 MAP2

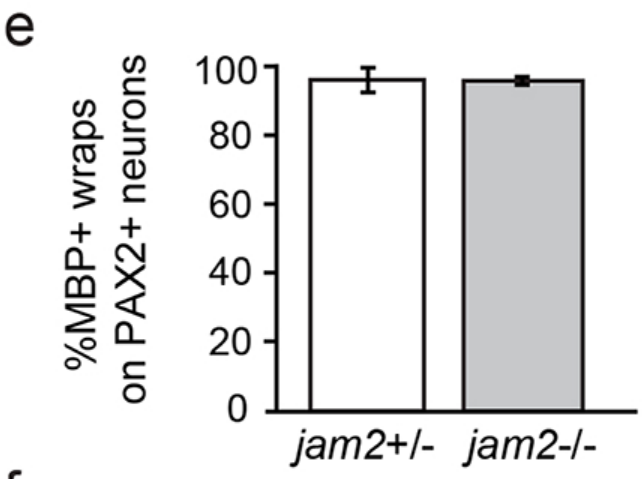
e
%MBP+ wraps on PAX2+ neurons
100
80
60
40
20
0
jam2+/-
jam2-/-

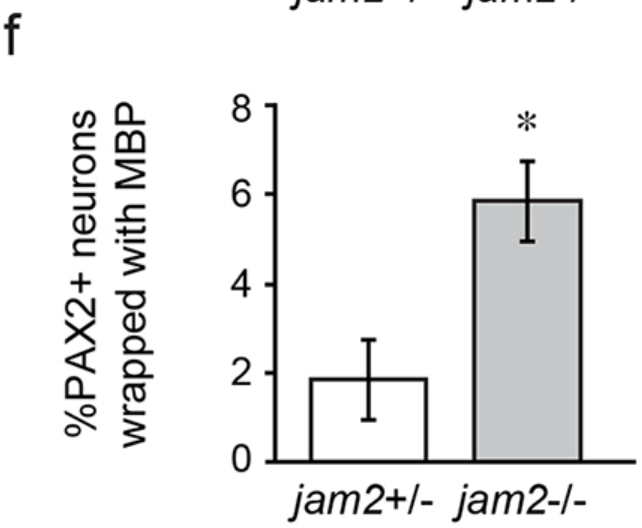
f
%PAX2+ neurons wrapped with MBP
8
6
4
2
0
*
jam2+/-
jam2-/-

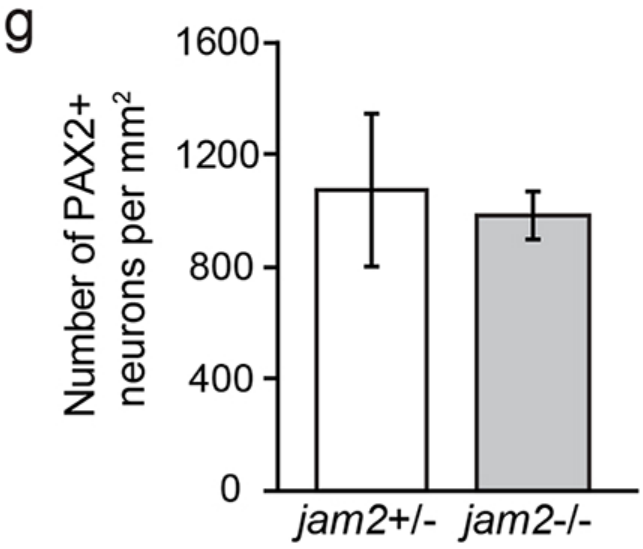
g
Number of PAX2+ neurons per mm2
1600
1200
800
400
0
jam2+/-
jam2-/-

Figure 8

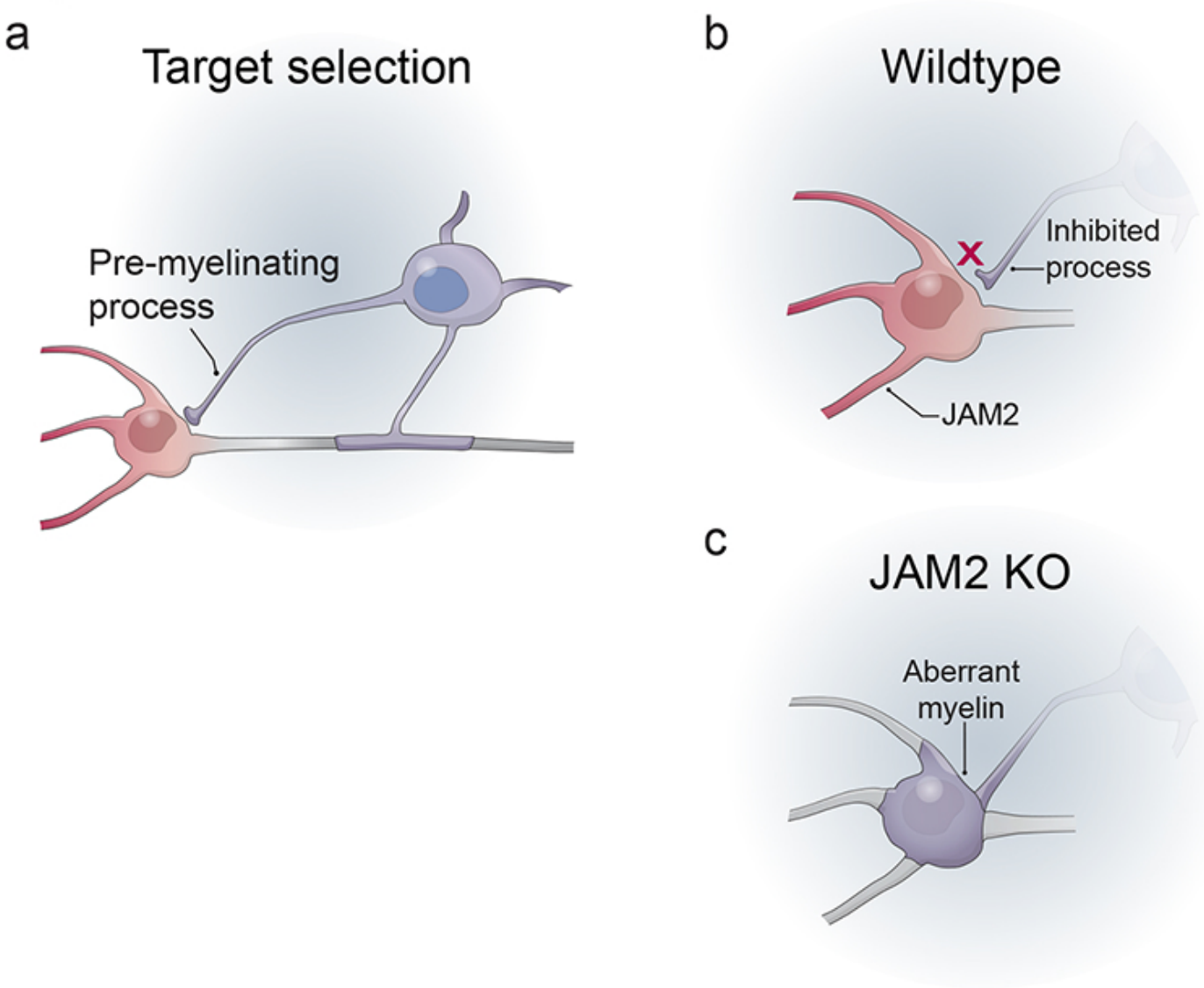
a
Target selection
Pre-myelinating process
b
Wildtype
X
Inhibited process
JAM2
c
JAM2 KO
Aberrant myelin

Figure S1

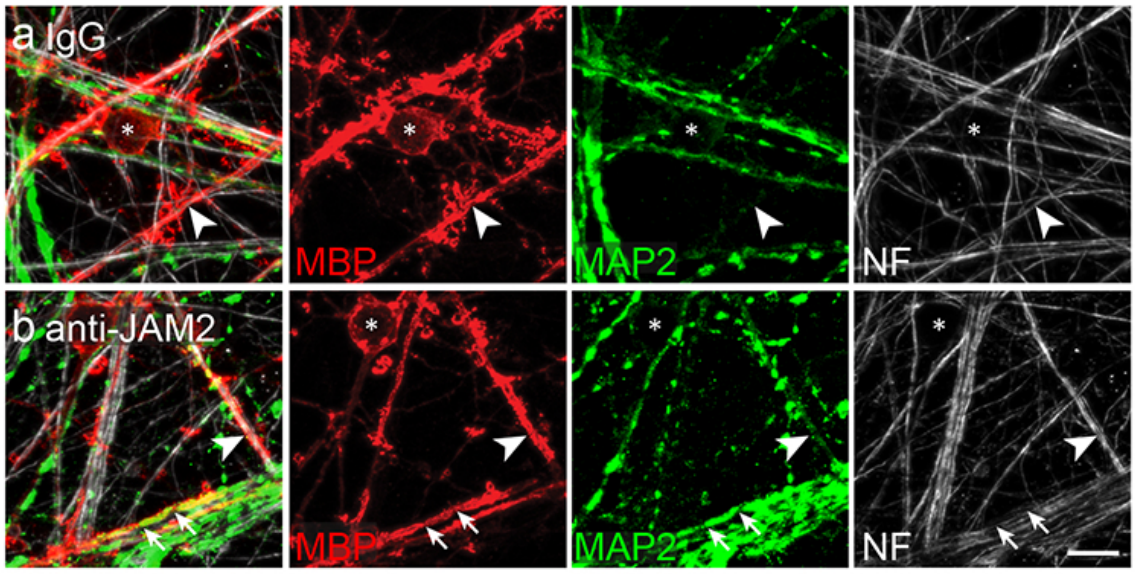
a IgG
MBP
MAP2
NF
b anti-JAM2
MBP
MAP2
NF

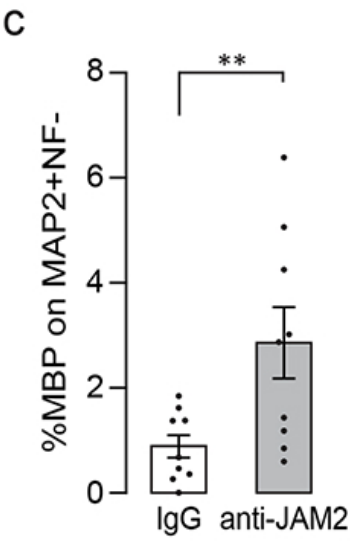
c
%MBP on MAP2+NF-
8
6
4
2
0
**
IgG
anti-JAM2

Figure S2

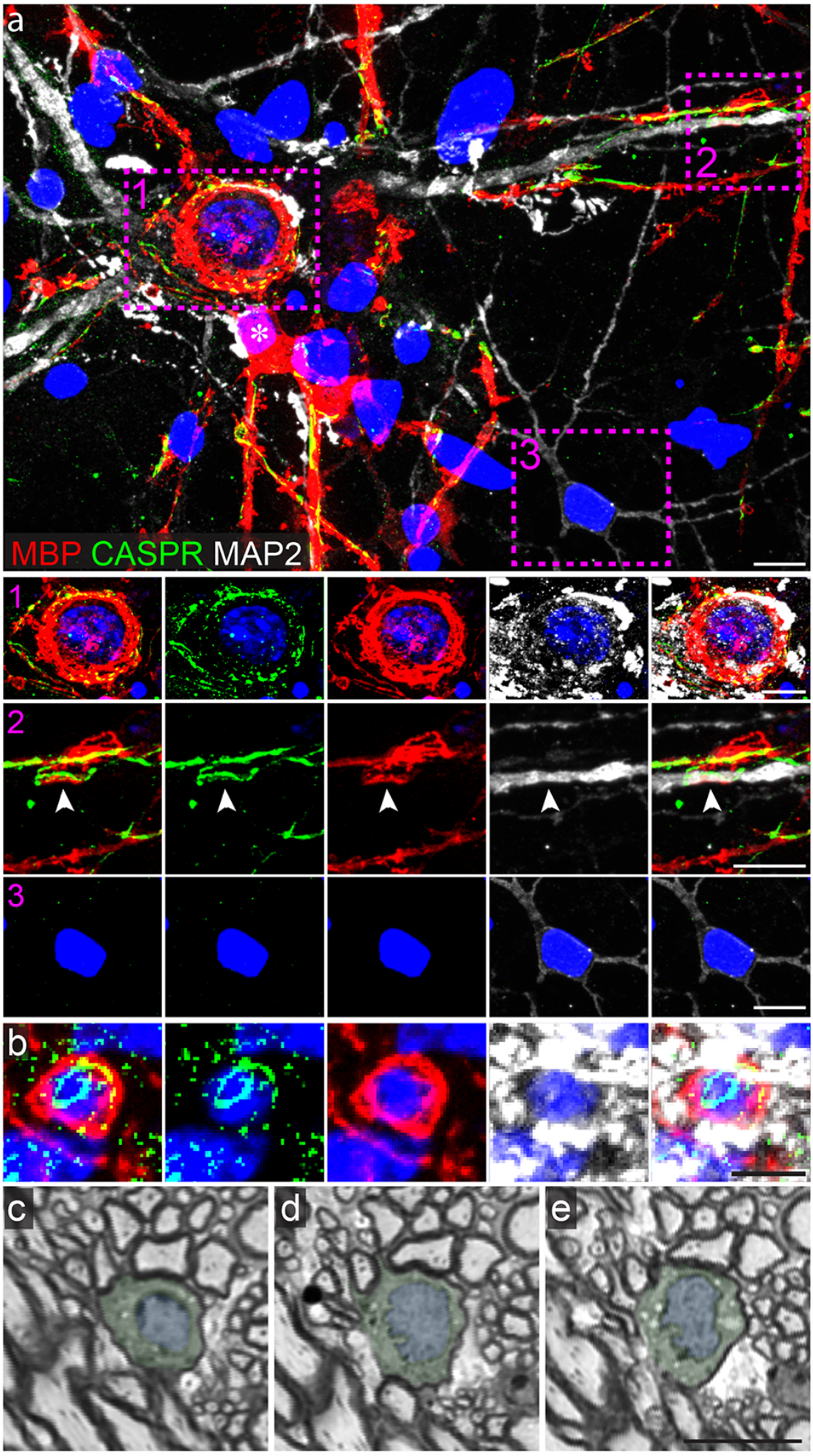

Figure S3

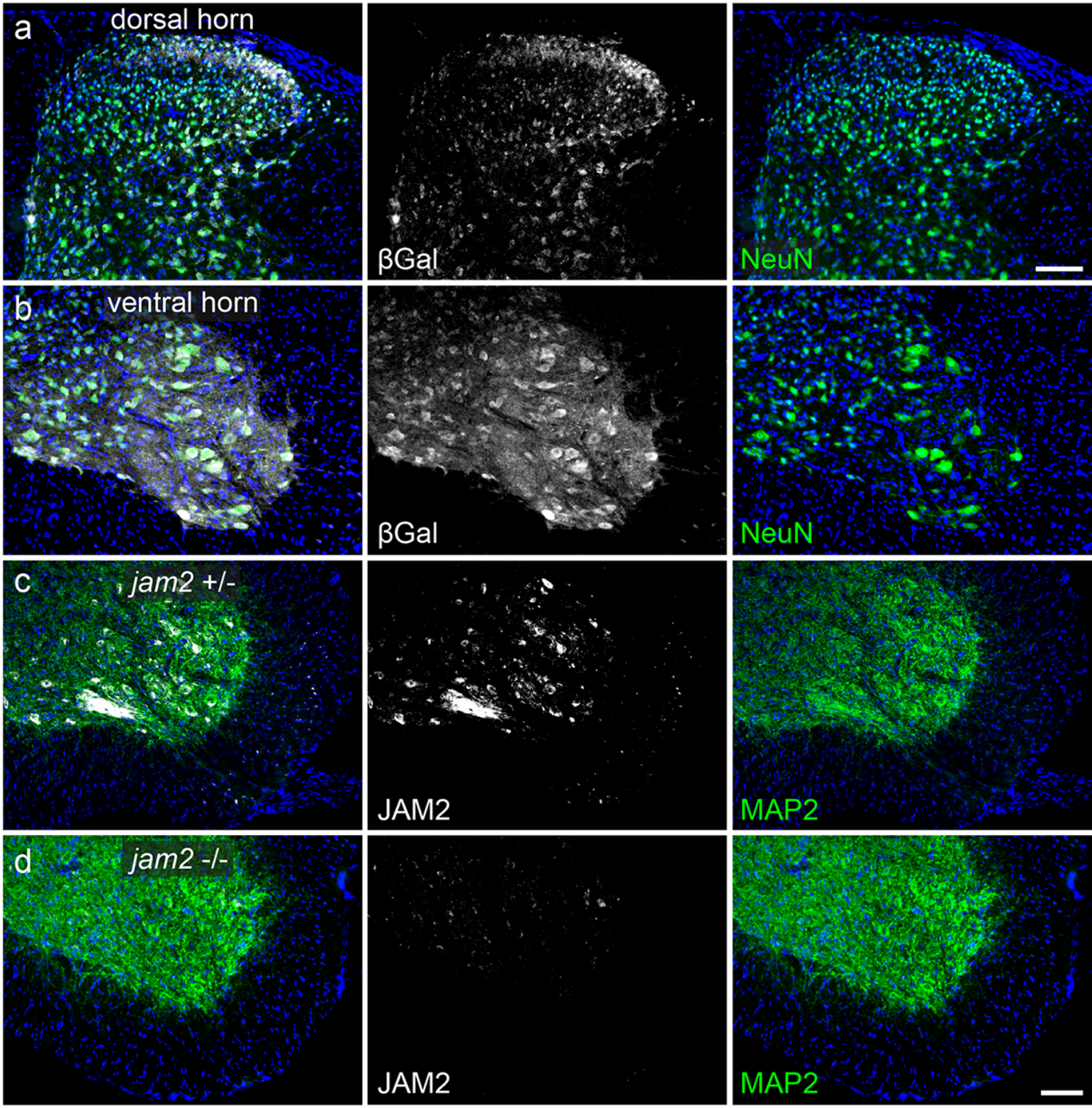
a
dorsal horn
βGal
NeuN
b
ventral horn
βGal
NeuN
c
jam2 +/-
JAM2
MAP2
d
jam2 -/-
JAM2
MAP2

Figure S4

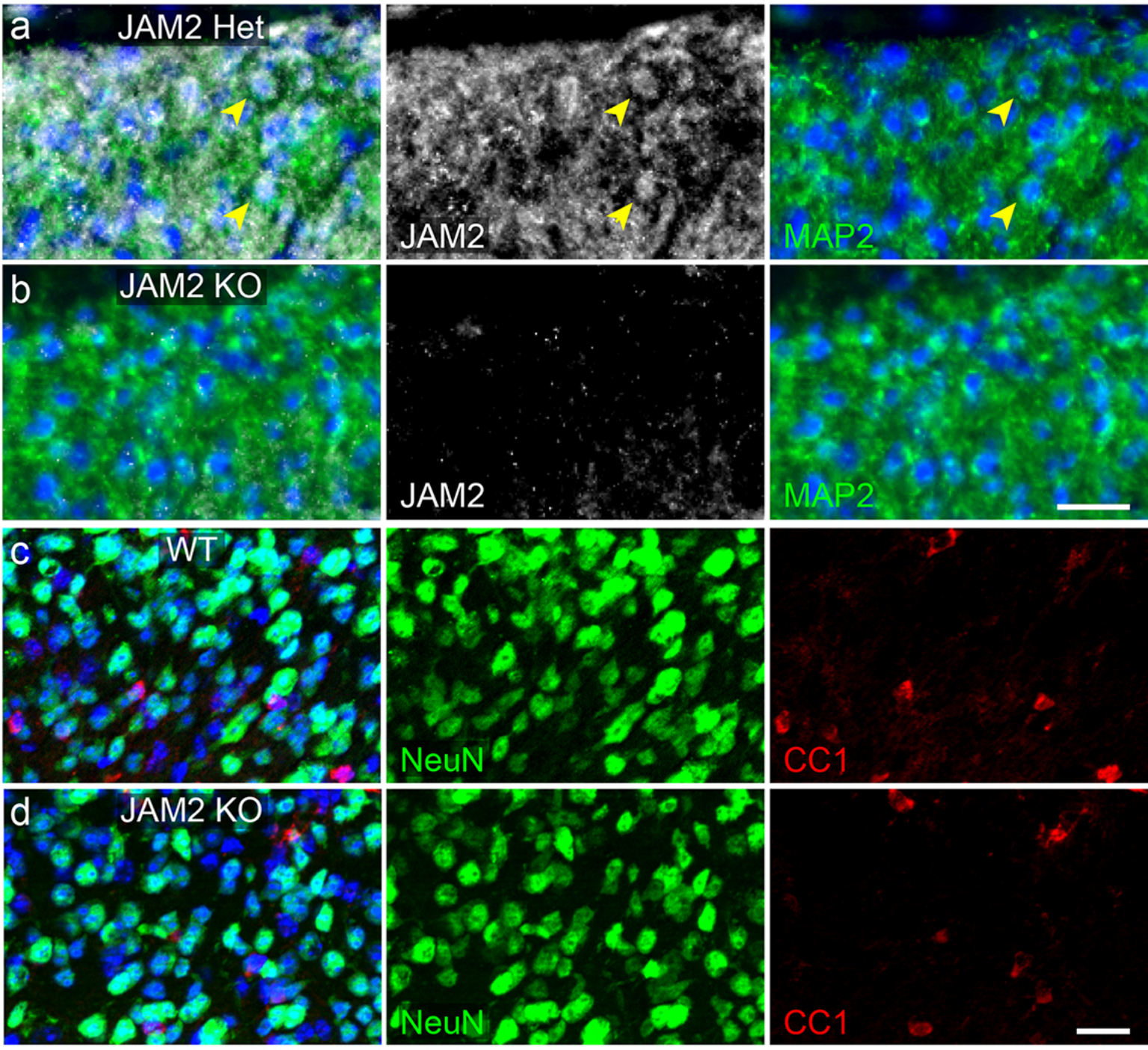
a
JAM2 Het
JAM2
MAP2
b
JAM2 KO
JAM2
MAP2
c
WT
NeuN
CC1
d
JAM2 KO
NeuN
CC1

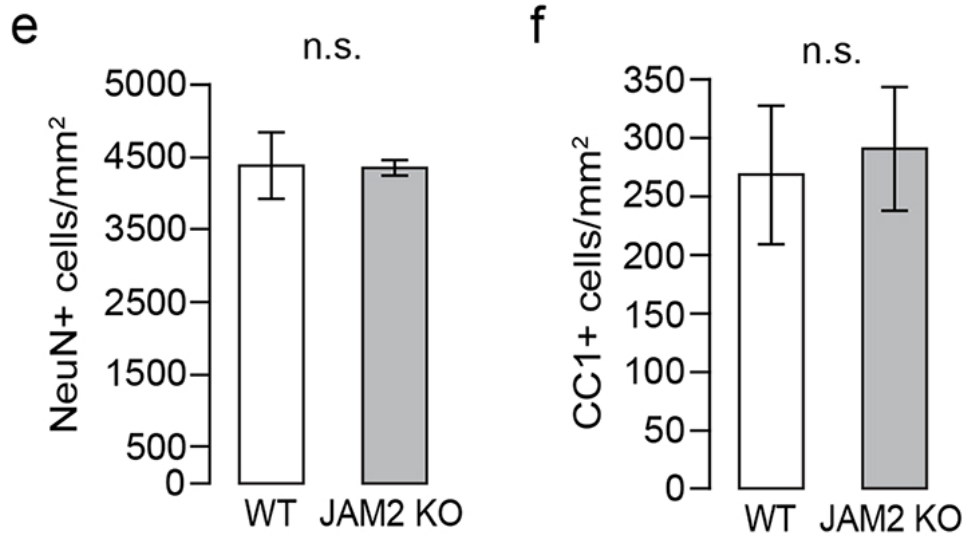
e
n.s.
NeuN+ cells/mm²
5000
4500
3500
2500
1500
500
0
WT
JAM2 KO
f
n.s.
CC1+ cells/mm²
350
300
250
200
150
100
50
0
WT
JAM2 KO

Figure S5

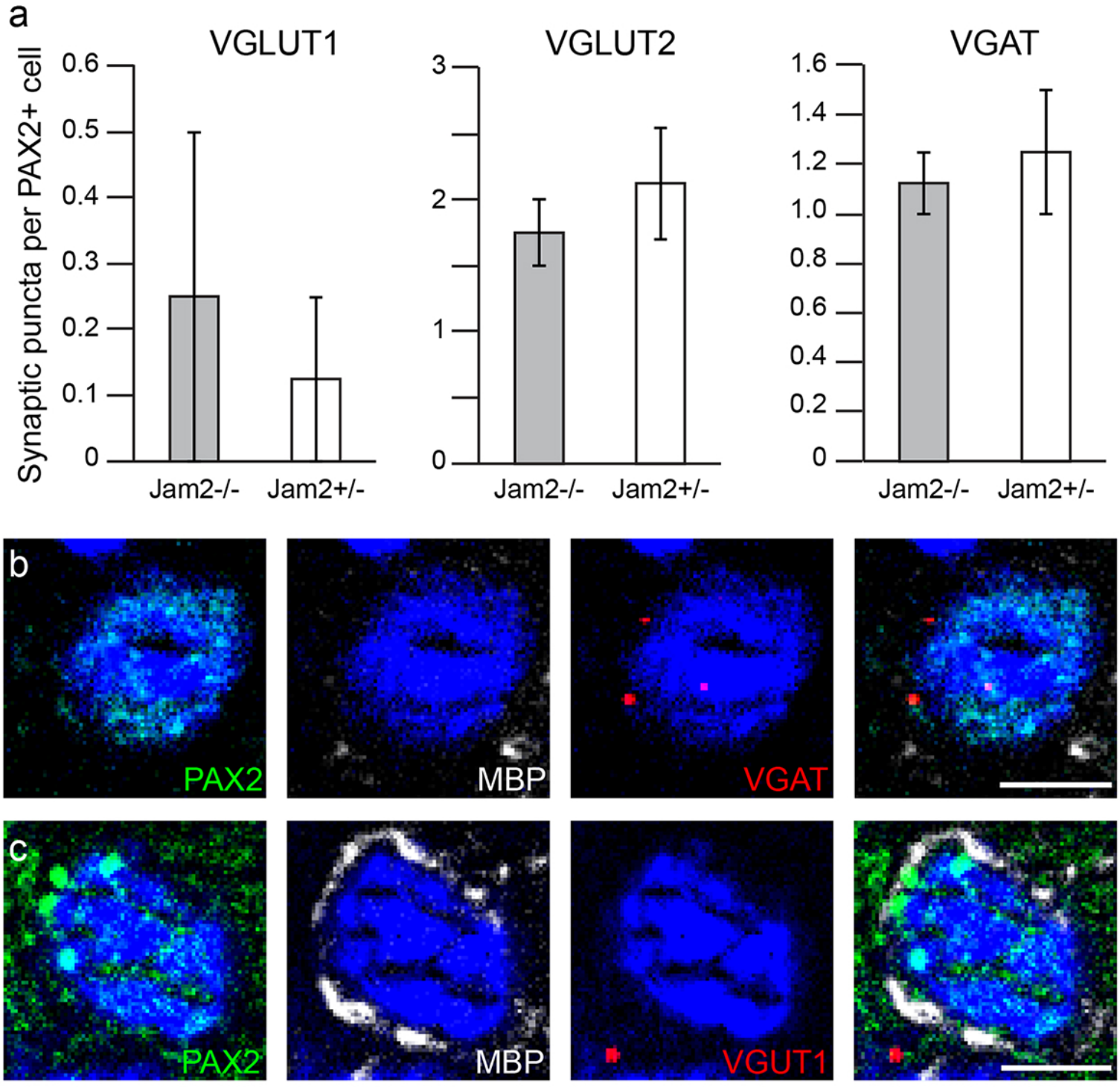
a
VGLUT1
VGLUT2
VGAT
Synaptic puncta per PAX2+ cell
0.6
0.5
0.4
0.3
0.2
0.1
0
3
2
1
0
1.6
1.4
1.2
1.0
0.8
0.6
0.4
0.2
0
Jam2-/-
Jam2+/-
Jam2-/-
Jam2+/-
Jam2-/-
Jam2+/-
b
PAX2
MBP
VGAT
c
PAX2
MBP
VGUT1